Electric Power Systems Research 237 (2024) 111025

Contents lists available at ScienceDirect

Electric Power Systems Research

journal homepage: www.elsevier.com/locate/epsr

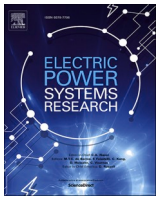

Highly sensitive protection scheme considering the PV operation control models

Feras Alasali [a], Hamza Albayadrah [a], Naser El-Naily [b], Hassen Loukil [c], William Holderbaum [d,*], Aymen Flah [e], Abdelaziz Salah Saidi [f]

[a] Department of Electrical Engineering, Faculty of Engineering, The Hashemite University, P.O. Box 330127, Zarqa 13133, Jordan
[b] College of Electrical and Electronics Technology-Benghazi, Libya
[c] Department of Electrical Engineering, College of Engineering, King Khalid University, Abha 61421, Saudi Arabia
[d] School of Science, Engineering and Environment, University of Salford, Salford, UK
[e] University of Business and Technology (UBT), College of Engineering, Jeddah, 21448, Saudi Arabia
[f] Université de Tunis El Manar, École Nationale d'Ingénieurs de Tunis, Laboratoire des Systèmes Électriques, Tunisie

ARTICLE INFO

Keywords:
Overcurrent relays
PV controllers
Optimal coordination
Distribution generation

ABSTRACT

The integration of distributed generation (DG) based on inverters into power systems has increased significantly, necessitating a thorough understanding of its impact on fault analysis and the performance of distribution networks' protection mechanisms. This study addresses this issue by examining how various inverter management modes influence protective relay systems within IEEE 9-bus redial and mesh networks, CIGRE and IEEE 33-bus networks featuring Photovoltaic (PV) farms and Battery Energy Storage Systems (BESS), by IEEE1547–2018 and German grid code standards. By analyzing grid-connected scenarios with five distinct PV control modes, the research introduces a novel protection methodology termed the Photovoltaic Overcurrent Relay (PVOCR). This method introduces a current-voltage characteristic to optimally coordinate Overcurrent Relays (OCRs), aiming to reduce their operational time and eliminate mis-coordination events. The proposed PVOCR is evaluated against standard inverse time, SOCR, and modern adaptive voltage, VOCR, relay schemes across various fault scenarios differing in type and location. Furthermore, the PVOCR scheme effectively operates across all PV inverter modes without experiencing miscoordination events, whereas the SOCR and VOCR schemes encountered such issues during the operation of Control 4. These results underscore the potential utility of the PVOCR methodology in enhancing the reliability and efficiency of protection systems in inverter-based DG networks.

1. Introduction

Renewable energy sources (RES) interfaced with power electronics referred to as converter-interfaced RESs are gaining popularity since they provide clean energy at a lower cost and have less fault contribution. As a result, increasing the use of RES is expected to not only change the dynamics of short circuit currents (SCC) but also result in the operation of power systems with lower fault levels [1,2], presenting a challenge to existing power system protection techniques [3,4]. During fault events, the behaviour of Inverter-Based Resources (IBRs) differs dramatically based on the internal logic control mechanisms. In addition, IBRs operate as grid-following systems, independent of control by the Distribution Network Operator (DNO) or consumer unit. They are commonly associated with variable renewable energy sources such as Photovoltaics (PV) and wind power. Consequently, predicting the behaviour of IBRs presents several challenges due to their association with fluctuating energy sources and lack of direct control by the distribution grid operator. Therefore, it is important to model power electronics inverters with current-limiting techniques to fully understand the network's transient fault response, ensure effective system protection, and avoid relay misoperations. The recent incorporation of IBRs into the DN presents difficulties for traditional protection systems in ensuring the grid's reliable and secure functioning. Because of the limited contribution of inverter currents during failures, the addition of IBRs affects fault currents in the system [5]. This change causes bidirectional current flows, which influence the protection system. Furthermore, if a significant number of inverters are incorporated into DNs, the rise in fault current levels may cause protective devices,

* Corresponding author.
E-mail address: w.holderbaum@salford.ac.uk (W. Holderbaum).

https://doi.org/10.1016/j.epsr.2024.111025
Received 17 May 2024; Received in revised form 3 August 2024; Accepted 25 August 2024
Available online 30 August 2024

particularly OCRs, which are often used in DNs for fault protection, to fail [3,4]. OCRs continuously monitor the current, and if it exceeds a preset limit, known as the pickup setting, the relay sends a trip signal to the circuit breaker. Increased IBR penetration has the potential to lower upstream fault currents below the pickup setting, impacting the reliability of standard protection methods [6]. In this work, an adaptive OCR protection scheme is designed and presented to overcome these challenges by considering the operation control model and limits of the Inverter-Based Distributed Generation (IBDG). The increasing integration of renewable energy into electrical networks over the last decade has had a considerable impact on protective systems. OCR-based protection systems have been found unsatisfactory for microgrids. Table 1 presents and summarizes the modern OCR protection schemes [7-27] for microgrid systems.

The literature presents various modern approaches to enhance the performance of OCRs in the context of evolving DG capabilities. The authors focus on the development of a unified set of relay settings applicable across using DG units, ranging from zero to the maximum required capacity. To tackle the protection coordination challenge, this methodology formulates the problem as a Linear Programming (LP) problem [11,14]. In another work, a hybrid tripping characteristic-based protection scheme for microgrids is presented, featuring fixed grading for relays independent of the mode of operation. This innovative approach eliminates the need for communication and significantly reduces relay operating times, particularly in low-fault-current situations during islanded mode [8]. Furthermore, different approaches are used in the direction of reactive power to discover and operation mode of the grid to determine the optimal OCR setting. In other works, by [11] and [15], OCR utilises an impedance-modulated harmonic current injection function, allowing each IBDG to have a separate harmonic component. This unique solution improves the protection scheme's directional element and overcurrent function. In addition, different time-current-voltage relay characteristics for OCRs are introduced in the context of meshed distribution networks with DG units [7]. This feature, which responds to the unique challenges provided by this network design, uses fault voltage magnitude and current to calculate OCRs' time of operation. In [8], the authors offer a communication-based dual time-current-voltage tripping characteristic for OCRs in gearbox systems of wind turbines. The proposed scheme provides two sets of settings, which are triggered based on the primary or backup mode of OCR operation, improving the adaptability of protective systems. Furthermore, [3,10] introduces a voltage–current inverse OCR model, demonstrating faster operating times compared to conventional OCR models for a power grid with DER at specific buses. Voltage and current phasors are used to calculate active and reactive power flow and determine a protection decision index. For power networks equipped with PV systems, the authors in [3,7] explore challenges to existing protection techniques, such as phase OCR and voltage-restrained OCR, and propose a modern method. This method involves setting pickup current as a function of positive sequence voltage for fault detection and determining the trip time from a three-dimensional trip characteristic in case of a fault.

The table highlights significant studies [15-20] that investigate optimizing protection schemes for IBDGs across various IEEE standard test systems and distribution networks. These studies employ a range of advanced optimization techniques such as nonlinear programming, genetic algorithms (GA), and meta-heuristic hybrids like Particle Swarm Optimization (PSO). Specifically, [20] employs an interior-point method to optimize standard overcurrent relays in the IEEE 30 test system. This approach aims to enhance the coordination and responsiveness of protection devices under varying grid conditions, ensuring effective fault detection and isolation. The work in [20] highlighted the important of

Table 1
Summary of the modern OCR schemes for power grid with grid-connected inverter.

Ref.	Year	Protection method	Test system	DG type	Optimization algorithms	Inverter control models limit
[7]	2014	time current-voltage characteristic	IEEE 30	IBDG	nonlinear programming	×
[8]	2015	communication-based time-current-voltage tripping characteristic	IEEE 24	DG	nonlinear programming	×
[9]	2018	local voltage and measurements technique	—-	IBDG	Genetic Algorithm (GA).	×
[10]	2019	voltage–current–time inverse-based protection	IEEE 30	IBDG	×	×
[11]	2020	a harmonic time-current-voltage directional relay	——	——	linear programming	×
[12]	2020	a local measurement-based protection	—-	IBDG	×	×
[13]	2020	a positive sequence relaying	IEEE 24	IBDG	×	×
[14]	2020	hybrid tripping characteristic	IEEE 14	SBDG	linear programming	×
[15]	2020	harmonic directional overcurrent relay	IEEE 9	IBDG	nonlinear programming	×
[16]	2021	quadrature (q) component	IEEE 14	IBDG	meta-heuristic hybrid	×
[17]	2021	nonstandard tripping characteristics	IEEE 9	IBDG	Particle Swarm (PSO) and GA.	×
[18]	2022	overcurrent and under/overvoltage	IEEE 14	IBDG	×	×
[19]	2022	voltage protection scheme	IEEE 33	IBDG	nonlinear programming	×
[20]	2022	standard overcurrent relay	IEEE30	IBDG	interior-point method	✓
[21]	2023	inverse time admittance relay	IEEE 69	IBDG	nonlinear programming	×
[22]	2023	non-standard characteristics- overcurrent relays	IEEE 30	IBDG	GA, cuckoo algorithm, and PSO	×
[23]	2023	time-current curve	IEEE14	IBDG	×	×
[24]	2023	voltage relay	IEEE 39	IBDG	×	×
[25]	2023	hybrid tripping characteristic	IEEE 33	IBDG	Vibrating Particles System algorithm (VPS)	×
[26]	2023	nonstandard current-voltage characteristics	IEEE 9	IBDG	GA	×
[27]	2023	a power-based integrated protection scheme	IEC-microgrid	IBDG	×	×
[28]	2023	dynamically adjusted the relay setting to accommodate varying operational conditions	EEE 6, 14 and 30-bus	—	Hybrid GA-NLP approach	×
[29]	2023	OCR group setting based on off-line and online artificial intelligence algorithms stages	IEEE 34	—	mixed-integer non-linear optimization algorithm	×
[30]	2023	dynamically adjusted the relay setting based on the penetration of DGs.	IEEE 33	—	radial basis function neural network	×
[31]	2023	time-voltage-current characteristics	IEEE 39	—	mixed-integer nonlinear programming	×
[32]	2023	The relay setting based on the worst-case conditions	DN	—	MILP solver	×
[33]	2024	pickup setting based on local voltage	IEEE 13	IBDG	Interior point optimization solver	×
	Proposed approach	positive sequence voltage -current characteristics	IEEE −9	IBDG	Water Cycle	✓

investigating and including the impact of the PV control mode during the design of the protection schemes. However, this study has primarily proposed fault detection methods that rely exclusively on current, which can present significant challenges for protection devices reliant on current-based detection to promptly identify all faults. While these methods may detect faults, they often suffer from extended tripping times, potentially impacting the overall reliability and efficiency of the protection scheme. Recently, the increasing integration of DGs, particularly those based on inverters, into power systems has led to significant challenges in power protection coordination. Adaptive protection schemes are essential in modern power systems due to their ability to dynamically adjust relay settings in response to changing network conditions, thereby enhancing reliability and operational efficiency. Tripathi and Mallik [28] presented an adaptive protection coordination strategy that utilizes user-defined characteristics for directional OCRs in microgrids. Their approach emphasizes flexibility and rapid response to network changes determined hybrid GA-NLP approach. This strategy is particularly beneficial in microgrids where the protection settings must be dynamically adjusted to accommodate varying operational conditions. However, the impact of the type of PV controllers was not investigated. Barranco-Carlos et al. [29] proposed an adaptive protection methodology for active distribution networks that combines fuses and relays with multiple setting groups. The use of multiple setting groups provides a practical means to achieve adaptive protection in real-time but without taking into account the different PV inverter contributions to the fault. Furthermore, Uma et al. [30] introduced an innovative adaptive overcurrent protection scheme using a radial basis function neural network. This method employed the learning capabilities of neural networks to predict and adjust relay settings in the occurrence of DG. The neural network model can quickly adapt to changes in the network, providing a robust solution without the need for lengthy optimization processes. The authors in [26,31] used voltage-dependent overcurrent relays in the contributing section. Zarour et al. [26], introduced an adaptive protection approach for using novel nonstandard current-voltage characteristics, enhancing the sensitivity and selectivity of protection systems in DG environments. Similarly, Assouak and Benabid [31] proposed a new coordination scheme for directional overcurrent protection relays that incorporates time-voltage-current characteristics, providing more reliable fault detection and isolation. For fault ride-through requirements, PV plants remain connected to the grid during faults, operating in different modes to meet grid demands [33]. The phase current from the PV plant during a fault matches the nominal current, limiting traditional phase current-based relaying methods. In [33] proposed a protection method using local positive sequence voltage and current, selecting pickup current via a current-voltage curve for fault detection and utilizing a three-dimensional time-current-voltage characteristic for trip time calculation. These studies highlighted the importance of integrating voltage and current signals to improve adaptive protection performance. However, the literature as summarized in Table 1 did not consider and investigate the impact of the control strategy of IBDG in terms of developing optimal and adaptive OCR schemes. Therefore, the control strategies of inverters based on the IEEE 1547 and grid code specifications [34] are considered in the designing of the proposed optimal adaptive OCR scheme. Overall, an adaptive protection scheme is a crucial solution proposed for networks incorporating solar energy. This approach is essential to address the dynamic changes in the network due to varying operational conditions. While traditional numerical overcurrent relays, such as Siemens SJ7 62 or Areva P132, have a limited number of groups (typically four), adaptive schemes can be utilized to select the appropriate group based on the grid operational mode, for example, grid-connected to PV, without PV or islanding mode [26-33], as described in Table 1. This literature did not investigate the impact of the control strategy of IBDG in terms of developing optimal and adaptive OCR schemes. The exclusion of PV inverter control mode from the protection scheme can lead to inadequate fault current limitation, reduced system stability, inefficient fault detection and isolation, increased risk of overcurrent, challenges in adaptive protection, and potential non-compliance with industry standards. Including this control mode is crucial for maintaining the reliability, stability, and safety of power systems with integrated renewable energy sources.

1.1. Contributions

As specified by IEEE1547 and grid code requirements and in [34], the protection system for distribution networks with IIDG faces several challenges, with inverter control playing an essential role in dealing with faults. The fault characteristics of renewable energy distribution networks affect traditional protection strategies. This study focuses on the contribution of fault currents from different PV) systems under five different control techniques for IIDG, highlighting the significance of developing adaptive OCR to deal with the effect of PV inverter control strategies and the variation of fault current contributions in IIDG systems. As a result, the main purpose of this article is to provide a timely examination of the issues associated with identifying challenges of developing optimal coordination schemes of OCR mechanisms inside emerging power systems. The emphasis is primarily on understanding the influence of various control strategies used in PV inverters. Considering the changing dynamics of power systems requires an assessment of these consequences for OCR protection and coordination. This paper's outlined contributions are as follows:

- Introducing and employing a new protection methodology (PVOCR) based on current-voltage characteristics that optimally coordinates OCRs, considering the different operation control modes of the smart grid-connected inverter compared to [26,31]. The aim is to minimize the operational time of OCRs without any instances of mis-coordination events over five different smart PV inverter control modes. In addition, the proposed scheme eliminates the need for communication and reduces costs associated with both communication infrastructure and computing.
- A comparative analysis of the proposed optimal coordination (PVOCR) traditional OCR (SOCR) and modern adaptive current-voltage (VOCR) [3,7] approach is conducted under different PV operation scenarios. This comparative analysis offers DN operators valuable initial insights into the potential influence of PV inverter control strategies on fault contribution and relay settings. These insights contribute to informed decision-making and assist in network planning.
- Early investigation of OCR protection challenges in modern and smart power systems, focusing on defect detection and coordination with an emphasis on the influence of diverse control techniques in PV inverters.

1.2. Outline of paper

The article is organized to address the research goals as follows: Section 2 provides the overview of the problem statement in terms of coordinating OCRs in modern power networks with IBDG. In Section 3, the proposed current-voltage protection schemes are described and illustrated. In Section 4, the simulation results and discussion are presented. Finally, the conclusions are discussed in section 5.

2. Problem statement: coordinating OCRs in modern power network with IBDG

Smart inverter control strategies have a vital role in the PV contribution during fault events, as highlighted by IEEE 1547 and grid code specifications. Fig. 1 presents the power distribution system that receives power from the main grid and IBDGs, distributing it through lines with OCRs. A failure at line 1, L1, results in fault current, F1, contribution entirely from the main grid in the case of the absence of the two

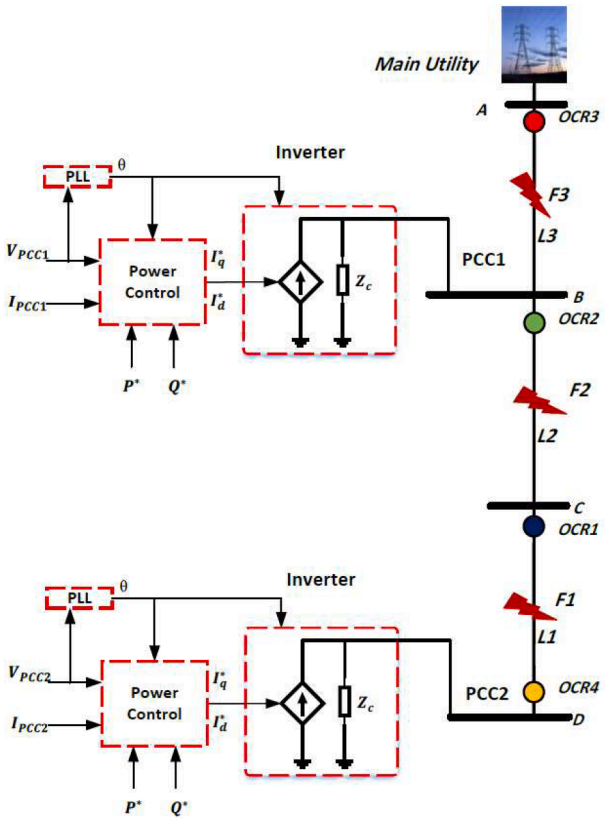

Fig. 1. Single line diagram of a power network connected to IBDG and OCRs.

PVs at PCC1 and PCC2. Where OCR1 will react with a primary protection action to protect the line L1, then OCR2 functions as a backup relay in the case of a delay or failure of OCR1, with Coordination Time Interval (CTI) considerations between the two relays. However, in the case of the two PV systems linked to the grid, the fault current contribution includes the main grid as well as PVs at PCC1 and 2. In general, the characteristics and contributions of the fault current will be determined by PV1 and PV2 inverter control strategies. In the environment of PV systems, control strategy selection and implementation from the main

Table 2
The current limits for the control strategies of IBDG.

Control strategy	IBDG contribution to fault current.	References and standards
Control 1	$I_{IBDG} = \begin{cases} 2\ 0 \le \lvert V_P^+\rvert \le 0.9 \\ 1\ 0.9 < \lvert V_P^+\rvert \le 1.1 \end{cases}$	Common inverter control [5,6]
Control 2	$I_{IBDG} = \begin{cases} 2\ 0 \le \lvert V_P^+\rvert \le 0.5 \\ -2.5.\lvert V_P^+\rvert + 3.25\ 0.5 < \lvert V_P^+\rvert \le 1 \\ 1\ 1 < \lvert V_P^+\rvert \le 1.1 \end{cases}$	German grid code [5],
Control 3	$I_{IBDG} = \begin{cases} 0\ 0 \le \lvert V_P^+\rvert \le 0.1 \\ 2\ 0.1 < \lvert V_P^+\rvert \le 0.5 \\ -2.5.\lvert V_P^+\rvert + 3.25\ 0.5 < \lvert V_P^+\rvert \le 0.8 \\ -1.\lvert V_P^+\rvert + 2\ 0.8 < \lvert V_P^+\rvert \le 1 \\ 0\ 1 < \lvert V_P^+\rvert \le 1.1 \end{cases}$	IEEE 1547–2018 [5,34],
Control 4	$I_{IBDG} = \begin{cases} 0.5\ 0 \le \lvert V_P^+\rvert \le 0.5 \\ -2.5.\lvert V_P^+\rvert + 3.25\ 0.5 < \lvert V_P^+\rvert \le 0.9 \\ 1\ 0.9 < \lvert V_P^+\rvert \le 1.1 \end{cases}$	IEEE 1547 standard [5, 34]
Control 5	$I_{IBDG} = \begin{cases} 0.5\ 0 \le \lvert V_P^+\rvert \le 0.5 \\ -2.5.\lvert V_P^+\rvert + 3.25\ 0.5 < \lvert V_P^+\rvert \le 0.9 \\ 1\ 0.9 < \lvert V_P^+\rvert \le 1.1 \end{cases}$	IEEE 1547 standard and ETAP [5,34]

five inverter control strategies, as described in Table 2, are critical in defining fault current contributions and impacting the overall performance of protection schemes. According to standards such as IEEE 1547–2018 and IEEE 2008–2022 [3,34], the inverter's requirements and constraints need to be taken into account. Initially, the fault current contribution from PV1 and PV2 is twice their full-rated current under the common and traditionally used inverter controller (method 1) for both Inverter 1 and Inverter 2. OCR1 and OCR4, as shown in Fig. 1, are added as primary protection relays, with OCR2 acting as a backup in the case of detection delays or failures. This concept increases investigation into advanced control techniques (2, 3, 4, and 5), which are currently common in practical applications and research, as shown in Table 2. Additionally, each control technique has different fault characteristics and contributions in the distribution systems, which require more advanced protection schemes to deal with these variations.

Analyzing the short-circuit current in a power network with IBDG is complex and challenging due to its nonlinear behaviour and dependence on the PV control strategies [5,6]. In general, the IBDG is a frequently utilized control technique that depends on the positive sequence voltage at the Point of Common Coupling (PCC) to mitigate the impact of voltage imbalance induced by short-circuit faults. An IBDG inverter system consists essentially of a DC voltage source, voltage source inverters, and filters, as shown in Fig. 1. The fault response of IBDG is highly impacted by the control approach used, with PQ control being extensively used in practice. Using a PQ-controlled current limiting approach aims to prevent the fault current in IBDGs from exceeding twice its rated value. In addition, to meet grid needs, IBDGs have Low Voltage Ride Through (LVRT) capabilities, allowing them to offer reactive power support. As a result, the current source of IBDG, I_{IBDG}, is controlled at PCC, as shown in Fig. 1, based on the positive sequence voltage at PCC, V_P^+, as described in Eq. (1). The fault current magnitude in IBDG is influenced by the renewable energy source, IBDG, through the variation of positive sequence voltage based on the behaviour of a control function, (f) [5,6]. This complexity makes it difficult to identify the faulty phase based on phase current magnitude only. Table 2 illustrates the influence of various inverter control modes, classified into five major IBDG control strategies.

$$I_{IBDG} = f\left(V_P^+\right) \tag{1}$$

The influence of different IBDG operating modes, categorized into five control groups in Table 2, on the fault current contribution of a PV plant is analyzed and presented in Fig. 2. The fault current contribution depends on the type of control used within the inverters, as each type reacts differently during a grid fault.

- Control 1: When the positive sequence voltage at PCC, V_P^+, ranges from 0.9 to 1.1 p.u, the current is regulated to 1.0 p.u (normal operating current). However, during fault conditions where V_P^+ drops below 0.9 p.u, this control limits the fault current to 2.0 p.u. This control strategy ensures that the fault current remains within defined limits based on V_P^+.
- Control 2: Following the German grid code [5], DGs within a microgrid need to have Low Voltage Ride Through (LVRT) capability. This capability allows DGs to support voltage levels during fault conditions by injecting reactive power. The fault current contribution of a PV, I_{IBDG}, is categorized into three distinct regions based on the V_P^+ level. The control mechanism for fault current regulation is such that when $V_P^+$is between 0.9 and 1.1 p.u, the current is limited to 1 p.u, as normal current. If V_P^+drops to between 0 and 0.5 p.u, I_{IBDG} is restricted to 2 p.u. Furthermore, this control strategy ensures fault current regulation for V_P^+set between 0.5 and 0.9 p.u by employing a linear relationship between the voltage and current, as described in Table 2. This approach ensures the stability and reliability of the system.

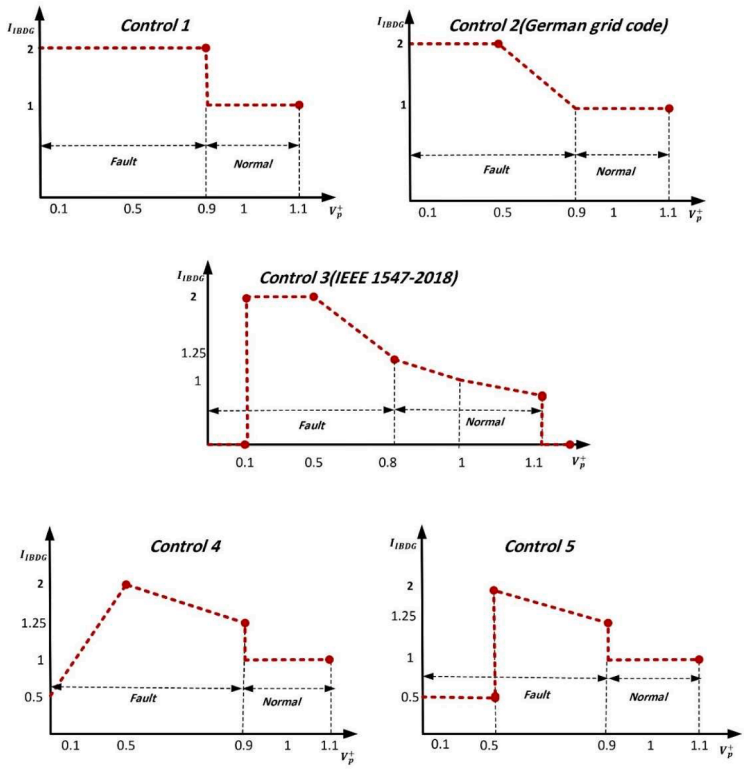

Fig. 2. The fault current contribution depends on the type of IBDG control.

- Control 3: According to IEEE 1547–2018 [5,34], this control strategy is employed to manage the fault current flow through five different stages.
  - When V_P^+ is between 0 and 0.1, I_{IBDG} is set to 0. This indicates that during fault operational conditions, no additional fault current is injected.
  - For V_P^+ ranging from 0.1 to 0.5, I_{IBDG} is fixed at 2. This represents a scenario where a moderate fault condition exists, and the IBDG injects a controlled amount of fault current.
  - V_P^+ between 0.5 and 0.8, the I_{IBDG} varies linearly according to the equation described in Table 2. This indicates a progressive reduction in fault current injection as the voltage increases, helping stabilize the system during partial fault conditions.
  - For V_P^+ between 0.8 to 1.1, the I_{IBDG} is defined by linear equations. This signifies that as the voltage continues to increase beyond 0.8 p.u, the fault current injection decreases further, thereby maintaining system stability. This control strategy ensures that the IBDG adapts its fault current contribution dynamically based on the voltage level at the V_P^+, thereby enhancing the stability and reliability of the microgrid system under varying grid conditions.
  - When $V_P^+ > 1.1$, I_{IBDG} is set to 0.
- Control 4: The current-limiting functionality of the inverter of control 4 is detailed in the IEEE 1547 standard [5,34]. The inverter's behaviour during fault conditions, normal generation, and shutdown was visually represented on the inverter's operation equations, as described in Table 2, offering a thorough understanding of its response.
  - When V_P^+ is between 0 and 0.5, the inverter current I_{IBDG} is limited based on a linear equation with a maximum value of 2 when V_P^+ is 0.5. This represents a low voltage scenario where the inverter contributes a minimal to the maximum amount of current.
  - For $0.5 < |V_P^+| \leq 0.9$, I_{IBDG} follows a linear relationship defined by the equation $-2.5.|V_P^+| + 3.25$. In this range, the inverter's current output decreases as the voltage increases, reflecting a controlled response to intermediate fault conditions.
  - When V_P^+ is between 0.9 and 1.1, I_{IBDG} is maintained at 1. This indicates that in normal operating voltage conditions, the inverter provides a stable current output.
- Control 5: In the IEEE 1547 standard and ETAP [5,34], the control strategy regulates fault current across three distinct areas:
  - When V_P^+ is between 0.9 and 1.1 p.u, the current is limited to 1 p.u.
  - If V_P^+ falls between 0.5 and 0.9 p.u, the fault current (I_{IBDG}) is constrained by a linear relationship with voltage: $-2.5.|V_P^+| + 3.25$.
- For $0 \leq |V_P^+| \leq 0.5$, the fault current is managed to be 0.5. This comprehensive control strategy allows for effective regulation of fault current, ensuring stability and reliability in various grid conditions.

2.1. The problem formulation of optimum OCRs coordination

The coordination challenge of OCRs in a DN with IBDGs has recently been presented as an optimization problem [3,4]. The primary goal of this optimization is to find the optimal OCR settings that minimize the tripping of OCRs while maintaining the selectivity and sensitivity between primary and backup OCRs. This section presents the mathematical formulation of the proposed optimization OCR coordination approach, designed to enhance the efficiency of OCR optimization strategies. To achieve this, an objective function ($T_{tripping}$) is introduced to minimize the total tripping time of primary and backup OCRs. The mathematical expression for the objective function is provided by Eq. (2) and detailed in [3].

$$T_{tripping} = \sum_{n=1}^{N} \sum_{s=1}^{S} t_{n,s} \tag{2}$$

Where the total tripping time of OCRs is $T_{tripping}$, $t_{n,s}$ is the tripping time

by relay (n) to operate when a fault occurs at location (s), and N and S are the total number of OCRs and total number of fault locations within the network. Considering these variables allows for evaluating the performance and efficiency of the OCR coordination strategy, specifically in terms of relay operational times at various fault locations across the distribution network. However, the formulation of the objective function ($T_{tripping}$) is subjected to a set of constraints. These constraints act as limitations or conditions for solving the optimization problem, ensuring the feasibility and validity of the optimization solution. Firstly, the selectivity constraint aims to determine the CTI (Coordination Time Interval) between primary and backup relays ($OCR_{primary}$ andOCR_{backup}), as described in Eq. (3). To ensure selectivity, the CTI is typically set within the range of 0.2 to 0.5 s, as recommended by the IEEE-242 standard. In this study, a CTI value of 0.3 s is used, which aligns with previous research [17]. Secondly, the minimum and maximum setting limitations for the tripping time (t_{min} and t_{max}) and the Time Multiplier Setting (TMS_{min} and TMS_{max}) at the OCRs, as described in Eqs. (4) and (5).

$$OCR_{backup} - OCR_{primary} \geq CTI \tag{3}$$

$$t_{min} \leq t_n \leq t_{max} \tag{4}$$

$$TMS_{min} \leq TMS_n \leq TMS_{max} \tag{5}$$

The tripping time of OCRs, $T_{tripping}$, o, as described in Eq. (2) for the SOCR scheme, is commonly defined using a standard inverse function [61–64]. In this study, two OCR characteristics are used as reference models. Firstly, the standard inverse OCRs characteristic, as described in Eq. (6) and described in the IEC 255–3, is a reference and commonly used scheme [4].

$$t_n = \left[\frac{A}{\left(\frac{I_{fault}}{I_{pickup}}\right)^B - 1}\right] TMS \tag{6}$$

where I_{fault} is the fault current, I_{pickup} is the pickup current, A and B are constantly determined according to established and employed OCR standards such as IEEE and IEC [17]. In this work, numerical OCRs following industry-standard IEC specifications are employed, with A and B values set at 0.14 and 0.02, respectively [35].

Secondly, adaptive OCR characteristics (VOCR), represented by Eq. (7) by [17], as an advanced and new scheme compared to inverse standard characteristics including the fault voltage term (V_{fault}) in the equation. This modern adaptive OCR including voltage term been employed to solve the modern DN protection challenges. The proposed nonstandard OCR characteristics incorporate a logarithmic function with constant (m) [3].

$$t_n = \left[\frac{A}{\left(\frac{I_{fault}}{I_{pickup}}\right)^B - 1}\right] \left(\frac{1}{e^{1-V_{fault}}}\right)^m TMS \tag{7}$$

3. The proposed current-voltage protection scheme

The proposed work stands out from traditional adaptive relaying methods because of its thorough investigation into how inverter control strategies affect fault conditions. While previous studies have explored various approaches to integrating solar energy into the grid, they often neglected to emphasize the specific types of control mechanisms employed by PV inverters. Traditional adaptive schemes typically prioritize adjusting relay settings in response to real-time changes in network conditions to maintain coordination among protection devices. However, these approaches are frequently exhibited by inverter-based resources under different control strategies, particularly during fault scenarios. In contrast, the proposed current-voltage protection scheme advances adaptive protection by integrating these control strategies directly into the protection framework. This ensures that the protection scheme not only responds dynamically to evolving network conditions but also optimizes its response based on the specific control modes implemented by PV inverters during faults. Moreover, while conventional adaptive techniques focus on modifying relay parameters such as pickup settings and time delays to manage dynamic changes in the network, they often do not fully address the unique fault characteristics introduced by inverter-based. The proposed work addresses this gap by explicitly analyzing and incorporating the behaviours of PV inverters under different control strategies. The previous discussion in Section 2 shows that there is a potential for using positive sequence components in addressing challenges related to protection based on phase current quantities. To tackle these challenges, this section introduces and employs an OCR scheme utilizing local positive sequence voltage and current for more efficient DN with PV systems [3,13]. In general, a short circuit in a power system can lead to a voltage drop. Consequently, there is the ability to utilize both voltage and current to detect the fault. The proposed approach suggests a current-voltage curve where the pickup current (I_{pick}) is a function of positive sequence voltage (V_P^+) [13], as in Eq. (8).

$$I_{pick} = 0.25\, U(V_P^+) + 1.5(V_P^+ - 0.25)U(V_P^+ - 0.25) \tag{8}$$

In this work, the pick current, I_{pick}, is directly affected and determined based on the positive sequence voltage, which is already used in the standard PV control to limit the current, as described in Table 2. This approach uses the positive sequence voltage to modulate the I_{pick} in response to voltage changes, ensuring that the overcurrent protection relays respond accurately to fault conditions. By incorporating voltage-dependent characteristics, this method enhances the protection system's sensitivity and selectivity, addressing the critical need for adaptive protection in DG environments. Eq. (8) includes $U(V_P^+)$ and $U(V_P^+ - 0.25)$ are unit step functions at 0 p.u and 0.25 p.u voltages, respectively. The proposed pickup current-voltage curve for fault detection is illustrated in Fig. 3. At the rated voltage, a current of 100 % of the maximum pickup current is necessary to activate the relay. As the input voltage decreases, the pickup current follows it, and at zero input voltage, 25 % of the maximum pickup current is required to operate the relay. Typically, the maximum pickup current in the distribution system is considered 150 % of the rated load current. Therefore, pickup current values are chosen as 0.25 p.u and 1.5 p.u at 0 p.u and 1 p.u voltages, respectively. A fault is confirmed when the magnitude of the positive sequence current exceeds the pickup current obtained for the positive sequence voltage from the curve.

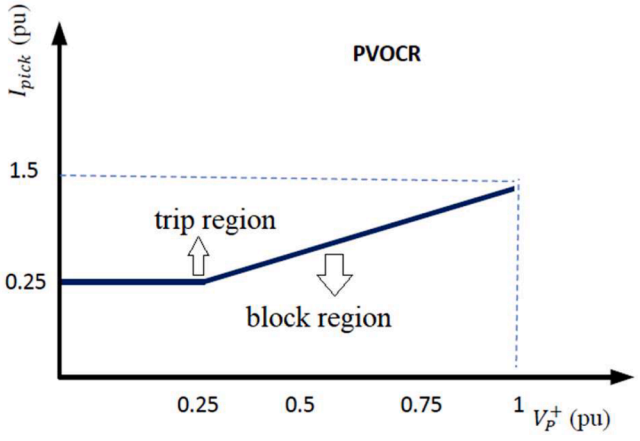

Fig. 3. The proposed pickup current curve based on the positive sequence voltage.

A fault is confirmed when the positive sequence fault current, I^{+}_{fault}, exceeds the pickup current, and the tripping time is determined using Eq. (9) for the proposed OCR scheme in this work (PVOCR). By employing the suggested three-dimensional time-positive sequence current-voltage characteristics to modify Eq. (7), Eq. (9) aims to minimize the impact of the PV control modes on the OCR scheme.

$$t_n = \left[\frac{A}{\left(\frac{I^{+}_{fault}}{0.25\ U\left(V^{+}_{P}\right)+1.5\left(V^{+}_{P}-0.25\right)U\left(V^{+}_{P}-0.25\right)} \right)^{B} - 1} \right] TMS \quad (9)$$

This approach will be named Voltage Restraint OCR (PVOCR), which aims to enhance the sensitivity of the OCR by adjusting its pickup current proportionally to the voltage, as shown in Fig. 3 and described by Eq. (7). Specifically, for V^{+}_{P} below 0.25 p.u, the OCR will trip at 25 % of its pickup value, and for voltages beyond 1 pu, the pickup current of the OCR will be 100 % of its pickup setting. To assess the performance of PVOCR compared to the standard inverse OCR scheme (SOCR) [3,17] and adaptive OCR based voltage term (VOCR) [3], a Single Line-to-Ground (SLG) fault at 50 % of the line connecting bus B and bus C is simulated in the system depicted in Fig. 4 under different fault resistances of 5, 10, and 15 Ω (F1, F2 and F3) to show the performance of the OCR schemes with minimum and maximum faults. The proposed PVOCR shows high performance over the three fault scenarios with minimum tripping time. In addition, the SOCR and VOCR faced a mis-operation event and did not detect the minimum fault scenario F3. In general, the existing protection techniques such as SOCR and VOCR for distribution systems have limitations in the presence of IDBG.

3.1. Optimization algorithms

In this section, the coordination problem of OCRs, as described in Eq. (9), in a distribution network equipped with IBDG is formulated as an optimization task with specific constraints. To address this coordination problem and minimize the tripping time of OCRs, the Water Cycle Optimization (WCA) is employed. The WCA has demonstrated effective performance in solving complex power network and protection problems [35]. The WCA is inspired by the natural water cycle and has been found to outperform standard optimization algorithms. The application of the WCA approach for microgrid protection coordination is described in previous works [35]. The WCA optimization process in this work is implemented using the MATLAB/SIMULINK toolbox. The WCA is used in our study to achieve a minimum tripping time for all OCRs (main and backup) by solving Eq. (9) while taking the relay constraints defined in Eqs. (3) to (5). Fig. 5 illustrates the general workflow of the solving process of the proposed OCRs coordination problem in this study. The initial step involves implementing the power network (IEEE 9 Bus with IDBG) and then performing a load flow analysis to establish the relay settings by determining the ratios of current transformers and plug settings for each OCR. Following this, short-circuit calculations based on IEC 60909 are conducted in various locations. Subsequently, the OCR system's optimal settings are derived using WCA for SOCR, VOCR and the proposed approaches PVOCR. The obtained settings' efficacy in the network protection scheme is then validated using ETAP software (Industrial Software). Through variations in the network's operating conditions and different inverter control strategies, the approaches are compared and tested.

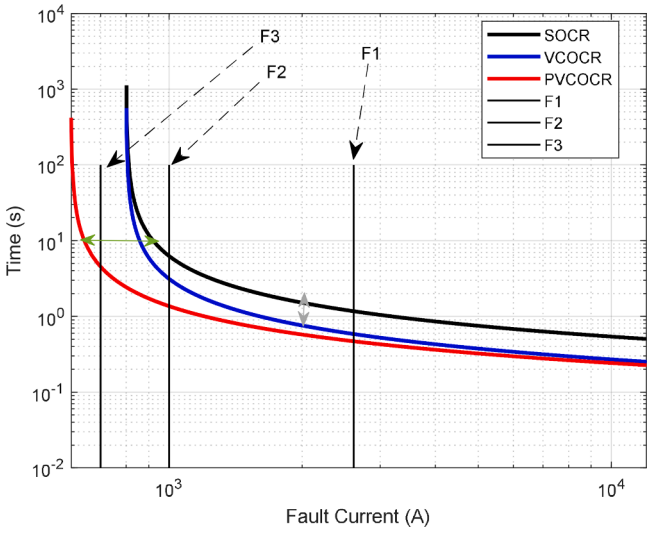

Fig. 4. The current-time characteristics for SOCR, VOCR and PVOCR under different fault scenarios.

4. Simulation results and discussion

The evaluation of the OCR protection schemes (SOCR, VOCR and PVOCR), as detailed in Section 3, involves testing on the IEEE 9 Bus distribution system with PVs and BESS. This section discusses the outcomes obtained through the utilization of the OCR protection schemes. Initially, the description of the system under study is presented, followed by the testing of the SOCR, VOCR and PVOCR under various power network fault scenarios (Three phase fault and single line to ground fault) in different locations. Throughout this section, a comparison is provided between the proposed PVOCR approach and the conventional standard inverse time scheme (SOCR) and modern adaptive voltage scheme (VOCR). The assessment includes a comparison of the overall

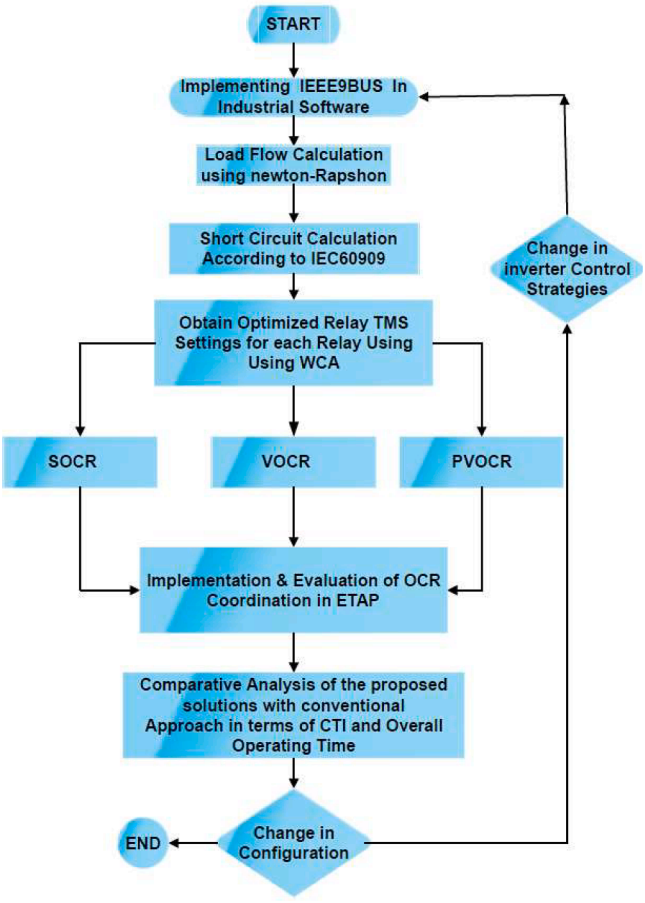

Fig. 5. General workflow of the optimal OCRs coordination approaches procedure implemented in this study.

operational time across different power network fault types and location scenarios. Finally, the effectiveness of the proposed PVOCR approach is evaluated using industrial software (ETAP), and the results are presented and compared with the SOCR and VOCR.

4.1. Power network description

The OCR coordination schemes are assessed on an IEEE 9 Bus test system equipped with PVs and BESSs systems, to optimize coordination and minimize overall operation time. The system, shown in Fig. 6, is modelled based on a radial system with a 9-bus feeder distribution system. This radial distribution system is supplied by a utility main source (20 MVA, 115/12.47 kV). Additionally, the distribution system incorporates two 7 MW Photovoltaic (PV) farms linked by a setup transformer rated at 0.4/12.47 kV, as detailed in references [17,35], where each 7 MW farm comprises ten 1 MW PV systems. The distribution network includes two 0.6 MW BESS systems connected to the grid via a setup transformer rated at 0.38/12.47 kV. The system includes 15 OCRs with current transformer ratio (CTR), as presented in Table 3, to deal with three-phase and single-line-to-ground faults over different locations (F1-F8), representing both near-end and far-end fault locations on each line. For each fault location, two primary OCRs are assigned, with each primary OCR having one backup OCR. For instance, in the event of a fault at F3, OCR3 operate as primary, while OCR4 serves as the backup relay. The OCR protection devices in Table 3 are initially configured based on a known operational state of the grid (common control mode, control 1). In our study, these OCRs were adjusted to align with specific operational states and inverter control types based on the voltage. Our proposed method performed excellently across all scenarios in terms of fault detection and response time. The proposed method allows for a unified configuration that adapts to different control modes of the IBDGs. This flexibility ensures that the system can handle various control modes simultaneously. In addition, if the DG is not of the IBDG type, our method still operates effectively. For instance, when adding a type like SGBDG, the fault current increases, and the protection device detects and isolates the fault faster than before. It is well known that fault currents in looped systems are smaller compared to radial systems. Consequently, the current passing through each protection device is lower in a looped system, resulting in longer trip times. However, with our proposed method, the trip time is reduced, ensuring faster fault isolation and improved system reliability.

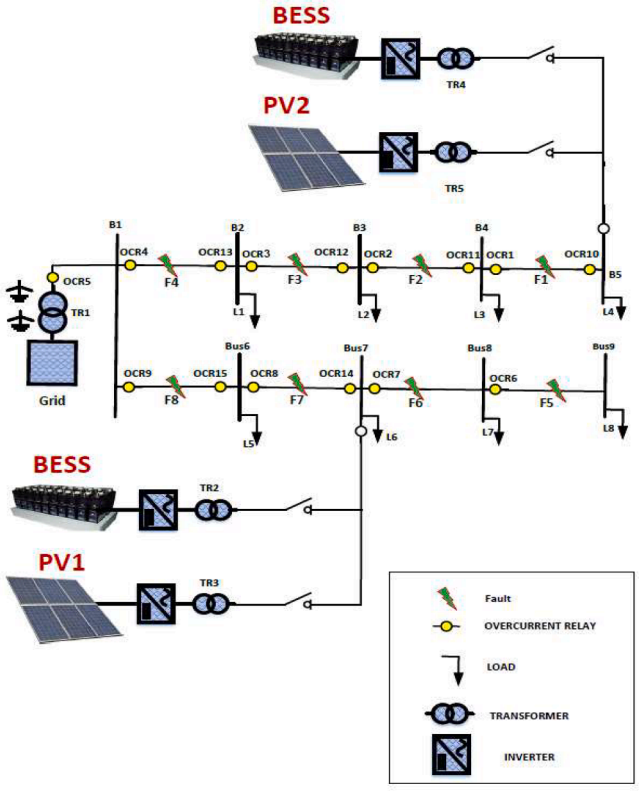

Fig. 6. IEEE 9 bus equipped with PV and BESS systems.

Table 3
The current transformer data for OCRs in the proposed power network.

OCR	CT ratio	Pickup current (A)
OCR 1 to 4	300/1	300
OCR 5	600/1	600
OCR 6 to 8	300/1	300
OCR 9	400/1	400
OCR 10 to 14	300/1	300
OCR15	400/1	400

4.2. PV voltage and current contribution results

In this section, the suggested OCR coordinating schemes are tested and evaluated over different fault scenarios in terms of locations and type. Firstly, the three-phase fault characteristics under five PV inverter control modes labelled Control 1, 2, 3, 4, and 5 are presented and evaluated. Table 4 provides a comprehensive overview of fault currents in various scenarios, including different fault locations, and PV control modes The results show distinct variations in fault currents based on fault locations and PV control modes. For instance, in Fault F3, under Control 4, OCR3 registered a lower fault current (5659 A) compared to other controls, where Control 5 registered a maximum current (6003 A). This variation in the contribution current from the PV inverter during fault based on the control model increases the challenge of developing an optimal OCR coordination scheme.

The PVs' contribution to fault currents is directly influenced by V_P^+ varying between PV system locations and control modes. Table 5 shows the V_P^+ results for both PV farms (PV1 and PV2) under different fault locations and inverter control modes. PV2 consistently

Table 4
The fault currents under different PV control modes and fault locations.

Fault location	Relays Pairs	Control 1	Control 2	Control 3	Control 4	Control 5
		Fault current (A)				
F1	OCR1	4693	4669	4669	4693	4693
	OCR2	4693	4669	4669	4693	4693
	OCR10	1125	**1000**	921	281	478
F2	OCR2	5253	5219	5215	5291	5289
	OCR3	5253	5219	5215	5291	5289
	OCR11	1125	1000	909	281	506
	OCR10	1125	1000	909	281	506
F3	OCR3	5991	5937	5922	5659	6003
	OCR4	5991	5937	5922	5659	6003
	OCR12	**1125**	1000	896	281	536
	OCR11	1125	1000	896	281	536
F4	OCR4	6849	6779	6753	6405	6739
	OCR5	6070	6089	6109	6248	6109
	OCR13	1125	997	884	281	569
	OCR12	1125	997	884	281	569
F5	OCR6	5332	5239	5184	4830	5174
	OCR7	5332	5239	5184	4830	5174
F6	OCR7	6019	5898	5838	5425	5808
	OCR8	5073	5062	5077	5256	5155
F7	OCR8	5956	5918	5911	5653	5972
	OCR9	5956	5918	5911	5653	5972
	OCR14	1125	1000	921	**281**	478
F8	OCR9	6839	6775	6748	6393	6678
	OCR5	6074	6092	6113	6251	6117
	OCR15	1125	1000	909	281	506
	OCR14	1125	1000	909	281	506

Table 5
The PV systems voltage (V_P^+) under different PV control modes and fault locations.

Fault location	Relays Pairs	Control 1 V_P^+ (p.u)	Control 2	Control 3	Control 4	Control 5
F1	PV1	0.1916	0.1612	0.1546	0.0479	0.0694
	PV2	0.6592	0.6442	0.644	0.6592	0.6592
	PV1	0.2192	0.1858	0.1749	0.0548	0.0877
	PV2	0.5766	0.5577	0.5544	0.5768	0.5766
F2	PV1	0.2192	0.1858	0.1749	0.0548	0.0877
	PV2	0.5766	0.5577	0.5544	0.5768	0.5766
	PV1	0.248	0.2115	0.1956	0.062	0.1086
	PV2	0.4915	0.4658	0.4548	0.3908	0.4916
F3	PV1	0.248	0.2115	0.1956	0.062	0.1086
	PV2	0.4915	0.4658	0.4548	0.3908	0.4916
	PV1	0.2775	0.2379	0.2164	0.0694	0.1326
	PV2	0.3679	0.3357	0.3184	0.2477	0.3403
F4	PV1	0.2775	0.2379	0.2164	0.0694	0.1326
	PV2	0.3679	0.3357	0.3184	0.2477	0.3403
	PV1	0.3061	0.2643	0.237	0.0769	0.1585
	PV2	0.2480	0.2115	0.1956	0.062	0.1089
F5	PV1	0.7021	0.6843	0.6837	0.6925	0.7017
	PV2	0.4297	0.4018	0.3876	0.3289	0.4203
F6	PV1	0.6202	0.5988	0.5954	0.6116	0.6171
	PV2	0.31	0.2804	0.2678	0.2047	0.2727
F7	PV1	0.5285	0.5052	0.4939	0.4063	0.5294
	PV2	0.1916	0.1612	0.1546	0.0479	0.069
	PV1	0.4254	0.3883	0.3620	0.2634	0.405
	PV2	0.2192	0.1858	0.1749	0.0548	0.0877
F8	PV1	0.4254	0.3883	0.3620	0.2634	0.405
	PV2	0.2192	0.1858	0.1749	0.0548	0.0877
	PV1	0.3061	0.2643	0.237	0.0769	0.1585
	PV2	0.2480	0.2115	0.1956	0.062	0.1089

demonstrates higher voltage compared to PV1 in fault locations (F1, F2, F3 and F4) as the PV system is near the fault location. On the other hand, PV1 shows higher voltage results compared to PV2 in fault locations (F5, F6, F7 and F8) as the PV system is near the fault locations. In Table 5, for Fault F1 under Control 1, PV1 registered V_P^+ (0.0479 p.u) compared to other controls, where Control 1 registered maximum voltage (0.19 p.u). While the PV2 for the same fault, PV2 registered V_P^+ (0.644 p.u) as lower voltage by using Control 3 compared to other controls, where Controls 1,4 and 5 registered maximum voltage (0.6592 p.u).

4.3. The optimal settings and the tripping time results for OCRs

To assess the performance of the suggested OCR protection schemes (SOCR, VOCR and PVOCR), as detailed in Section 3, optimal OCR settings were determined for the proposed power network fed by both a utility feeder, two PV systems and two BESS, as shown in Fig. 5. Firstly, Table 6 provides a comprehensive result of the optimal OCR settings for the SOCR, VOCR and PVOCR under three-phase fault condition and different PV inverter control modes. Secondly, the comparison between the OCR schemes (SOCR, VOCR and PVOCR) term of total tripping time is presented in Table 6, specifically focusing on the tripping times for primary and backup OCR pairs during three-phase faults. The proposed PVOCRS approach demonstrates high performance, achieving minimum tripping time compared to the benchmark SOCR and VOCR approaches PV inverter control 1 and 5 modes. For example, the overall tripping time for SOCR, VOCR and PVOCR is 16.13, 15.12 and 13.67 s during Control 1 mode. However, the VOCR approach outperforms the PVOCR when the Control 2, 3 and 4 modes are employed. In general, the overall tripping time term does not provide a clear image of the performance of the proposed OCR schemes under each fault scenario.

The evaluation of OCRs schemes, comparing SOCR and VOCR against the positive voltage OCR approach (PVOCR), was conducted over different fault locations (F1 to F8) under different inverter control modes. The tripping times for primary and backup OCR pairs during faults are presented in Tables 7 and 8. In general, the PVOCR approach demonstrates superior performance, achieving minimum tripping times compared to the benchmark SOCR scheme overall fault scenarios and outperforming VOCR in the case of minimum faults. However, the VOCR outperformed PVOCR during the number of fault scenarios in terms of primary OCR reaction. For example, the VOCR registered tripping time equal to 0.3 s during F2 at OCR2 compared to 0.35 s for PVOCR. The effectiveness of the PVOCR scheme was shown within the operating overall PV inverter modes without any miscoordination events. The SOCR and VOCR faced miscoordination events during the PV operation using Control 4, as shown in Table 7.

Additionally, this section compares the suggested PVOCR approach to the traditional scheme (SOCR) during the new type of fault (single line to ground fault). Table 9 shows the tripping times of the OCRs over different fault locations. The PVOCR shows high performance compared to SOCR without any miscoordination event and minimum tripping time. The SOCR approach registered two events of mis coordination at SOCR11 and 14. this indicates potential vulnerabilities in the traditional SOCR scheme, emphasizing the need for a more efficient protection

Table 6
The TMS and overall tripping time results under different PV control modes.

OCR	Control 1			Control 2			Control 3			Control 4			Control 5		
	TMS														
	SOCR	VOCR	PVOCR	SOCR	VOCR	PVOCR	SOCR	VOCR	PVOCR	SOCR	VOCR	PVOCR	SOCR	VOCR	PVOCR
OCR 1	0.010	0.010	0.010	0.010	0.010	0.010	0.010	0.010	0.010	0.010	0.10	0.010	0.010	0.010	0.010
OCR 2	0.1715	0.7021	0.249	0.1712	0.702	0.249	0.171	0.708	0.249	0.1715	0.702	0.249	0.171	0.702	0.296
OCR 3	0.339	1.197	0.453	0.339	1.201	0.453	0.339	1.2045	0.453	0.340	1.195	0.453	0.340	1.195	0.492
OCR 4	0.516	1.499	0.626	0.5149	1.508	0.626	0.514	1.515	0.626	0.513	1.527	0.626	0.518	1.497	0.659
OCR 5	0.514	3.067	0.7485	0.515	1.795	0.751	0.516	1.801	0.752	0.530	3.257	0.767	0.519	3.00	0.780
OCR 6	0.010	0.010	0.010	0.010	0.010	0.010	0.010	0.010	0.010	0.010	0.01	0.010	0.010	0.010	0.010
OCR 7	0.179	0.970	0.249	0.178	0.688	0.249	0.177	0.688	0.249	0.170	1.028	0.251	0.175	0.689	0.252
OCR 8	0.335	1.521	0.443	0.334	1.143	0.444	0.335	1.143	0.445	0.337	1.601	0.452	0.335	1.147	0.448
OCR 9	0.462	1.679	0.571	0.459	1.324	0.572	0.460	1.322	0.573	0.458	1.770	0.579	0.460	1.321	0.576
OCR 10	0.239	2.351	0.627	0.219	1.209	0.627	0.200	1.209	0.6261	0.130	0.130	0.626	0.111	0.688	0.642
OCR 11	0.163	1.97	0.453	0.149	0.825	0.453	0.136	0.825	0.453	0.090	0.090	0.453	0.081	0.491	0.465
OCR 12	0.086	1.579	0.250	0.079	0.426	0.250	0.072	0.426	0.249	0.050	0.05	0.249	0.0476	0.265	0.255
OCR 13	0.010	0.01	0.010	0.010	0.010	0.010	0.010	0.01	0.010	0.010	0.010	0.010	0.010	0.010	0.010
OCR 14	0.089	1.577	0.250	0.0828	0.439	0.251	0.077	0.439	0.250	0.050	4.0	0.250	0.0523	0.230	0.250
OCR 15	0.010	0.010	0.010	0.010	0.010	0.010	0.010	0.010	0.010	0.010	0.01	0.010	0.010	0.010	0.010
Overall operational time (S.)	16.137	15.128	13.678	16.185	12.144	13.685	16.232	12.451	13.683	16.610	12.775	13.725	17.44	14.37	14.12

Table 7
The tripping time results for SOCR and VOCR schemes under different PV control modes.

Fault Location	Relays Pairs	Control 1		Control 2		Control 3		Control 4		Control 5	
		Operational tripping time for OCR (second)									
		SOCR	VOCR	SOCR	VOCR	OCR	VOCR	SOCR	VOCR	SOCR	VOCR
F1	OCR1	0.025	0.004	0.025	0.004	0.025	0.005	0.025	0.004	0.025	0.004
	OCR2	0.425	0.404	0.425	0.404	0.425	0.408	0.425	0.405	0.425	0.404
	OCR10	1.253	1.775	1.26	0.999	1.254	1.066	No tripping	No tripping	1.661	1.433
F2	OCR2	0.408	0.306	0.408	0.306	0.408	0.309	0.407	0.306	0.407	0.520
	OCR3	0.808	0.706	0.808	0.707	0.808	0.709	0.807	0.706	0.930	0.885
	OCR11	0.852	1.493	0.856	0.680	0.854	0.735	No tripping	No tripping	1.079	0.910
	OCR10	1.253	1.894	1.259	1.056	1.254	1.136	No tripping	No tripping	1.479	1.310
F3	OCR3	0.771	0.519	0.772	0.521	0.772	0.523	0.788	0.519	0.772	0.519
	OCR4	1.171	0.919	1.172	0.922	1.172	0.925	1.188	0.919	1.177	0.919
	OCR12	0.455	0444	0.456	0.351	0.458	0.384	No tripping	No tripping	0.572	0.444
	OCR11	0.852	1.592	0.856	0.721	0.866	0.784	No tripping	No tripping	0.972	0.844
F4	OCR4	1.120	0.653	1.121	0.657	1.122	0.660	1.138	0.664	1.131	0.652
	OCR5	1.520	1.054	1.521	1.061	1.522	1.061	1.547	1.064	1.532	1.765
	OCR13	0.052	0.002	0.058	0.008	0.064	0.009	No tripping	0.002	0.118	0.015
	OCR12	0.452	0.402	0.458	0.373	0.464	0.409	No tripping	No tripping	0.518	0.415
F5	OCR6	0.024	0.003	0.024	0.004	0.024	0.004	0.018	0.003	0.018	0.004
	OCR7	0.424	0.403	0.424	0.405	0.424	0.404	0.418	0.403	0.418	0.405
F6	OCR7	0.406	0.261	0.406	0.299	0.407	0.299	0.401	0.267	0.402	0.299
	OCR8	0.806	0.661	0.806	0.701	0.807	0.699	0.801	0.667	0.802	0.699
F7	OCR8	0.762	0.408	0.763	0.496	0.765	0.496	0.781	0.422	0.761	0.498
	OCR9	1.168	0.808	1.163	0.898	0.849	0.896	1.181	0.823	1.161	0.898
	OCR14	0.467	1.190	0.467	0.362	0.476	0.387	No tripping	No tripping	0.783	0.481
F8	OCR9	1.109	0.506	0.076	0.637	0.808	0.636	1.127	0.520	1.114	0.635
	OCR5	1.519	1.052	0.476	1.060	1.521	1.060	1.165	1.062	1.531	1.758
	OCR15	0.067	0.002	1.106	0.011	0.085	0.012	No tripping	0.002	0.297	0.041
	OCR14	0.467	0.403	1.520	0.384	0.485	0.412	No tripping	0.926	3.076	0.441

Table 8
The tripping time results for the PVOCR scheme under different PV control modes.

Fault location	Relays Pairs	Control 1	Control 2	Control 3	Control 4	Control 5
		Operational time for OCR (second)				
		PVOCR	PVOCR	PVOCR	PVOCR	PVOCR
F1	OCR1	0.014	0.014	0.0140	0.014	0.014
	OCR2	0.414	0.414	0.4140	0.414	0.491
	OCR10	0.881	0.853	0.882	0.880	0.902
F2	OCR2	0.351	0.351	0.351	0.351	0.416
	OCR3	0.751	0.751	0.751	0.751	0.816
	OCR11	0.637	0.637	0.637	0.637	0.641
	OCR10	1.039	1.039	1.037	1.037	1.041
F3	OCR3	0.637	0.637	0.637	0.637	0.692
	OCR4	1.037	1.037	1.0371	1.037	1.092
	OCR12	0.351	0.351	0.351	0.351	0.352
	OCR11	0.582	0.751	0.751	0.751	0.752
F4	OCR4	0.879	0.879	0.879	0.879	0.926
	OCR5	1.258	1.279	1.279	1.279	1.326
	OCR13	0.014	0.014	0.014	0.014	0.0137
	OCR12	0.414	0.414	0.414	0.414	0.414
F5	OCR6	0.018	0.014	0.014	0.0184	0.018
	OCR7	0.414	0.414	0.414	0.416	0.418
F6	OCR7	0.351	0.351	0.351	0.353	0.354
	OCR8	0.737	0.751	0.751	0.753	0.754
F7	OCR8	0.622	0.624	0.625	0.636	0.63
	OCR9	1.023	1.024	1.025	1.036	1.030
	OCR14	0.352	0.352	0.352	0.569	0.351
F8	OCR9	0.857	0.859	0.860	0.869	0.864
	OCR5	1.253	1.279	1.279	1.278	1.322
	OCR15	0.014	0.015	0.014	0.015	0.014
	OCR14	0.389	0.416	0.414	0.415	0.415

system. These findings highlight the need to use the suggested PVOCR technique for power system protection as a more reliable and sensitive solution, particularly in an environment of increasing use of PV inverters in the network with different control scenarios.

Table 9
The tripping time results for PVOCR and SOCR scheme under single line to ground fault.

Relay	V_p^+ (p.u)	Fault current	Tripping time
SOCR3	0.7511	5659	0.7877
PVOCR3			0.7157
SOCR11	0.7125	281	Not operate
PVOCR11			2.2967
SOCR4	0.7542	6405	1.138
PVOCR4			1.039
SOCR14	0.7213	281	Not operate
PVOCR14			1.33
SOCR5	0.7632	6251	1.313
PVOCR5			1.119

4.4. Discussion and comparison using ETAP

In this section application of a standardized computer program (ETAP) extends to evaluating the OCRs coordination problems and changes within the distribution system with PV and BESS, focusing specifically on the impact of using different inverter control modes. The main focus of this investigation is the coordination of OCRs within the system depicted in Fig. 6 through:

- Evaluation of OCR Coordination: The section underscores the use of ETAP to simulate and evaluate the coordination of OCRs within a system incorporating both PV and BESS. This evaluation is crucial for understanding how different inverter control modes affect the overall coordination of protection schemes.
- Visualization of Results: Figs. 7–9 in the section provide a visual representation of the Time-Current Characteristic (TCC) curves for different OCRs (PVOCR, VOCR, and SOCR) across various fault locations and inverter scenarios. These visualizations are essential for demonstrating the effectiveness of the proposed coordination scheme under different operational conditions.

To achieve optimal coordination, a simulation model is developed

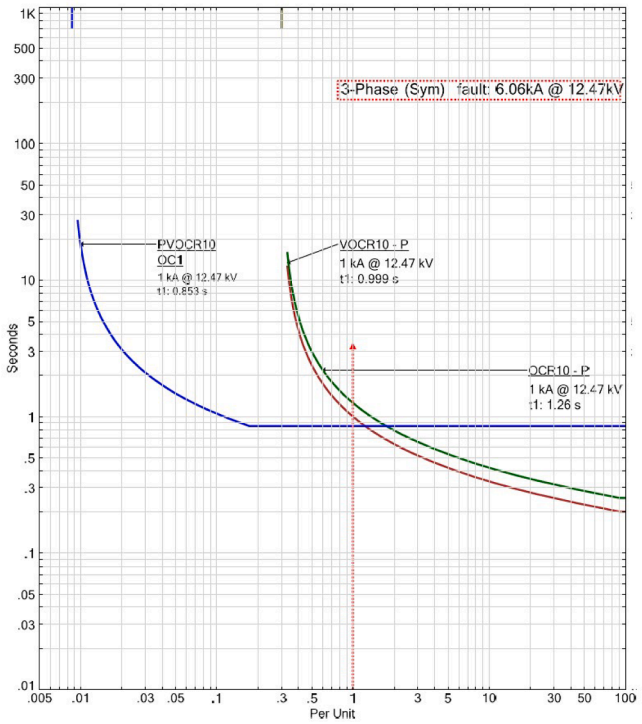

Fig. 7. The TCC curves for PVOCR, VOCR and SOCR of OCR 10 when a fault occurs at location F1 and Control 2 for the PV inverter.

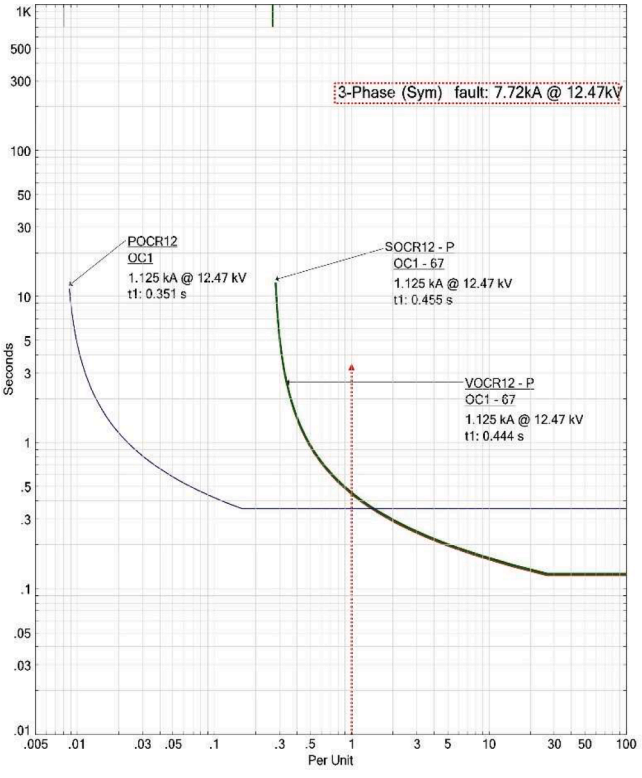

Fig. 8. The TCC curves for PVOCR, VOCR and SOCR of OCR 12 when a fault occurs at location F3 and Control 1 for the PV inverter.

utilizing ETAP. Additionally, the WCA algorithm is employed to solve the coordination problem in the OCR schemes. The results of ETAP are presented in Figs. 7–9. These figures aim to show the time-current characteristic curves (TCC) of PVOCR, VOCR and SOCR across the

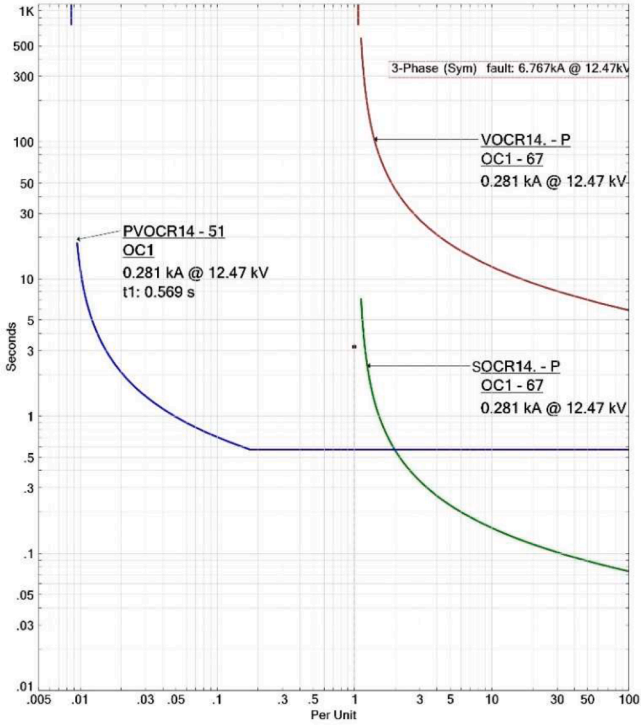

Fig. 9. The TCC curves for PVOCR, VOCR and SOCR of OCR 14 when a fault occurs at location F7 and Control 4 for the PV inverter.

different fault locations and inverter scenarios.

- Fig. 7 shows the TCC curves for the proposed OCR schemes (PVOCR, VOCR and SOCR) of OCR 10 when a fault occurs at location F1 and Control 2 for the PV inverter. The PVOCR 10 operates first (0.853 s), followed by the VOCR with 0.999 s and finally, SOCR 10 with 1.26 s. Additionally, the PVOR approach outperformed the VOCR and SOCR during fault (F3) and Control 1 for the PVs scenario, as shown in Fig. 8. The PVOCR recorded the minimum tripping time for OCR 12 with 0.351 s compared to 0.444 and 0.455 s for VOCR and SOCR, respectively.
- At the minimum fault current level, the VOCR and SOCR faced challenges in detecting the faults. For example, at fault location (F7) and Control 4 for the inverter control scenario, the VOCR14 and SOCR14 did not operate the were not able to detect the fault of 281 A. While the PVOCR was able to detect it within an operational time equal to 0.569 s.

4.5. *Large-scale power system*

In this section, a larger network system is employed to assess the proposed adaptive coordination scheme and to test its applicability to other distribution networks.

- CIGRE distribution network

To address coordination issues, a CIGRE distribution network with DG, as described in [25]. This evaluation aims to validate the scheme's effectiveness and transferability across different network configurations. The CIGRE grid is supplied by a utility HV/MV source and protected by 14 OCRs. Additionally, this grid is connected to two 5 MVA PV units via a 1/20 kV step-up transformer, as detailed in previous works [25]. The required OCR data to simulate the CIGRE network model are listed in Table 10.

The evaluation of OCR schemes, comparing SOCR and VOCR against the Positive Voltage OCR approach (PVOCR), was conducted across

Table 10
The CT ration at the CIGRE grid.

Relay	CT Ratio
OCR1	50
OCR2	50
OCR3	50
OCR4	50
OCR5	200
OCR6	200
OCR7	50
OCR8	50
OCR9	50
OCR10	50
OCR11	50
OCR12	50
OCR13	300
OCR14	300

various fault locations (F1 to F14) under different inverter control modes. Tripping times for primary and backup OCR pairs during faults are presented in Tables 11 and 12.

In general, the PVOCR approach demonstrated superior performance, consistently achieving minimum tripping times compared to the benchmark SOCR scheme across all fault scenarios. PVOCR also outperformed VOCR in most cases, indicating its effectiveness in minimizing fault clearance times. However, VOCR exhibited faster tripping times in certain fault scenarios for primary OCR reactions. For example, VOCR tripped in 0.273 s at OCR3 during F3, compared to 0.45 s for PVOCR. The effectiveness of the PVOCR scheme was further highlighted by its operation across all PV inverter modes without any miscoordination events. This reliability contrasts with SOCR, which faced miscoordination events during PV operations under Control 3 and 4, as detailed in Table 12. Overall, the results underscore the robust performance of PVOCR in optimizing OCR coordination for PV-integrated distribution networks. Its ability to minimize tripping times and avoid miscoordination events makes it a promising approach for enhancing the reliability and efficiency of protection systems in the presence of distributed generation.

- IEEE 33-Bus network

This section utilizes a larger distribution network model, the IEEE 33-bus system, to evaluate and compare the SOCR and VOCR against the PVOCR scheme. The goal is to demonstrate the transferability and effectiveness of the PVOCR scheme to other distribution networks. Fig. 10 illustrates the IEEE 33-bus system, where each bus voltage is constrained to within 10 % of its nominal value. The network is supplied by the utility system and includes two 4-MW solar power plants. Table 13 shows the initial TMS for each OCR in the IEEE 33-bus system. By employing three phase fault, the study aims to validate the PVOCR scheme's performance and demonstrate its applicability to diverse distribution networks under Control 4 for the PV systems.

Tripping times for primary and backup OCR pairs during faults are detailed in Table 14. The performance of different protection schemes was evaluated under various fault locations and Control 4.

- The PVOCR scheme consistently demonstrated superior performance, achieving the shortest tripping times across all faults when compared to the SOCR and VOCR.
- PVOCR also outperformed the VOCR, indicating its efficiency in reducing fault clearance times.
- The reliability of the PVOCR scheme was highlighted by its consistent operation without any miscoordination events., as shown in Table 14.
- The results highlight the effectiveness of the PVOCR approach in minimizing fault clearance times and ensuring reliable protection coordination across various PV inverter modes.

In addition, Table 15 presents the tripping times for primary and backup OCR pairs during faults under the other PV controllers. The performance of different protection schemes was evaluated all fault locations. The PVOCR scheme outperformed VOCR and SOCR schemes and demonstrated high performance, achieving the shortest tripping times across all faults. Tables A1–A4 in Appendix A showed the detailed optimal setting for all schemes and under different PV controllers. The results highlighted the effectiveness of the PVOCR approach in minimizing fault clearance times and ensuring reliable protection coordination across various PV inverter modes.

Fig. 11 illustrates the convergence behavior of three different algorithms: SOCR, VOCR, and PVOCR, with the y-axis representing overall operation time and the x-axis representing the number of iterations.

Table 11
The tripping time results for SOCR and VOCR schemes under different PV control modes at the CIGRE network.

Fault location	Relays Pairs	Control 1		Control 2		Control 3		Control 4		Control 5	
		Operational time for OCR (second)									
		SOCR	VOCR	SOCR	VOCR	SOCR	VOCR	SOCR	VOCR	SOCR	VOCR
F1	OCR1	0.029	0.006	0.019	0.001	0.020	0.0014	0.028	0.001	0.024	0.001
	OCR2	0.329	0.306	0.319	0.301	0.320	0.301	0.328	0.301	0.324	0.301
F2	OCR2	0.326	0.265	0.315	0.260	0.317	0.291	0.327	0.274	0.322	0.291
	OCR3	0.626	0.566	0.615	0.660	0.617	0.591	0.627	0.536	0.622	0.591
F3	OCR3	0.609	0.377	0.598	0.434	0.558	0.146	0.621	0.406	0.568	0.273
	OCR4	0.909	0.677	0.898	0.734	0.858	0.446	0.921	0.608	0.868	0.573
F4	OCR4	1.116	0.694	1.104	0.748	1.056	0.457	1.294	0.656	1.074	0.588
	OCR5	1.416	0.994	1.410	1.048	1.356	0.757	1.594	1.573	1.374	0.888
F5	OCR5	1.297	0.708	1.290	0.743	1.244	0.543	1.530	1.495	0.991	0.276
	OCR6	1.597	1.00	1.596	1.043	1.552	0.843	1.830	2.535	1.291	0.660
F6	OCR6	1.245	0.466	1.249	0.474	1.215	0.382	0.736	0.355	1.011	0.300
F7	OCR7	0.019	0.002	0.016	0.002	0.016	0.002	0.0164	0.002	0.016	0.002
	OCR8	0.319	0.302	0.316	0.302	0.316	0.306	0.316	0.314	0.316	0.302
F8	OCR8	0.308	0.160	0.304	0.157	0.338	0.153	0.311	0.214	0.305	0.236
	OCR9	0.021	0.465	0.606	0.457	0.639	0.454	0.611	0.549	0.605	0.536
F9	OCR9	0.021	0.419	0.591	0.328	0.628	0.360	0.407	0.502	0.538	0.233
F10	OCR10	0.0194	0.003	0.019	0.002	0.019	0.002	0.029	0.091	0.022	0.002
F11	OCR11	0.021	0.820	0.017	0.004	0.017	0.004	0.0182	1.072	0.025	0.022
	OCR12	0.321	1.120	0.318	0.304	0.317	0.304	0.318	1.526	0.325	0.322
F12	OCR12	0.295	1.015	0.282	0.194	0.283	0.194	0.290	1.045	0.179	0.076
F13	OCR13	0.301	0.103	0.070	0.005	No tripping	1.114	No tripping	1.195	0.219	0.004
F14	OCR14	0.072	0.103	0.075	0.002	0.075	0.002	No tripping	0.00	0.988	1.303

Table 12
The tripping time results for PVOCR schemes under different PV control modes at the CIGRE network.

Fault location	Relays Pairs	Control 1	Control 2	Control 3	Control 4	Control 5
		Operational time for OCR (second)				
		PVOCR	PVOCR	PVOCR	PVOCR	PVOCR
F1	OCR1	0.009787405	0.009812188	0.00979479	0.009784554	0.009787405
	OCR2	0.309787419	0.309812236	0.309786207	0.346865404	0.309787418
F2	OCR2	0.289787288	0.28984076	0.30569726	0.324451453	0.305792614
	OCR3	0.589787762	0.589841612	0.605705795	0.624840251	0.605792666
F3	OCR3	0.476239419	0.474654748	0.354111394	0.504608527	0.450555686
	OCR4	0.776239886	0.774656559	0.654111448	0.804610263	0.75055668
F4	OCR4	0.859741507	0.858095359	0.724528122	0.89150631	0.878674434
	OCR5	1.159741558	1.158095376	1.02452822	1.191507329	1.178674435
F5	OCR5	1.012278547	1.009104974	0.896892066	1.140840483	0.721064177
	OCR6	1.31227967	1.309106281	1.197023552	1.440840498	1.021065999
F6	OCR6	0.94391713	0.94143844	0.860834603	0.476061967	0.734260386
F7	OCR7	0.01291585	0.011741789	0.011649748	0.009580342	0.011167305
	OCR8	0.313199486	0.311741835	0.311650011	0.309580425	0.311172145
F8	OCR8	0.242697965	0.241538304	0.241449147	0.239878702	0.287987748
	OCR9	0.54342244	0.541734204	0.541590982	0.539879781	0.020225271
F9	OCR9	0.52162551	0.459443809	0.480106102	0.472456927	0.015527042
F10	OCR10	0.013134727	0.013135058	0.013135058	0.010849121	0.013135794
F11	OCR11	0.013897511	0.01382155	0.013820791	0.013822092	0.024897153
	OCR12	0.3138224	0.313821564	0.313824494	0.3139423	0.324897231
	OCR12	0.287340558	0.267693393	0.268559058	0.276089461	0.159689788
F12	OCR13	0.15402886	0.026857975	0.026762903	0.026846792	0.026874009
F13	OCR14	0.027034749	0.015671988	0.015666931	0.015666089	0.027095656
F14	OCR1	0.009787405	0.009812188	0.00979479	0.009784554	0.009787405

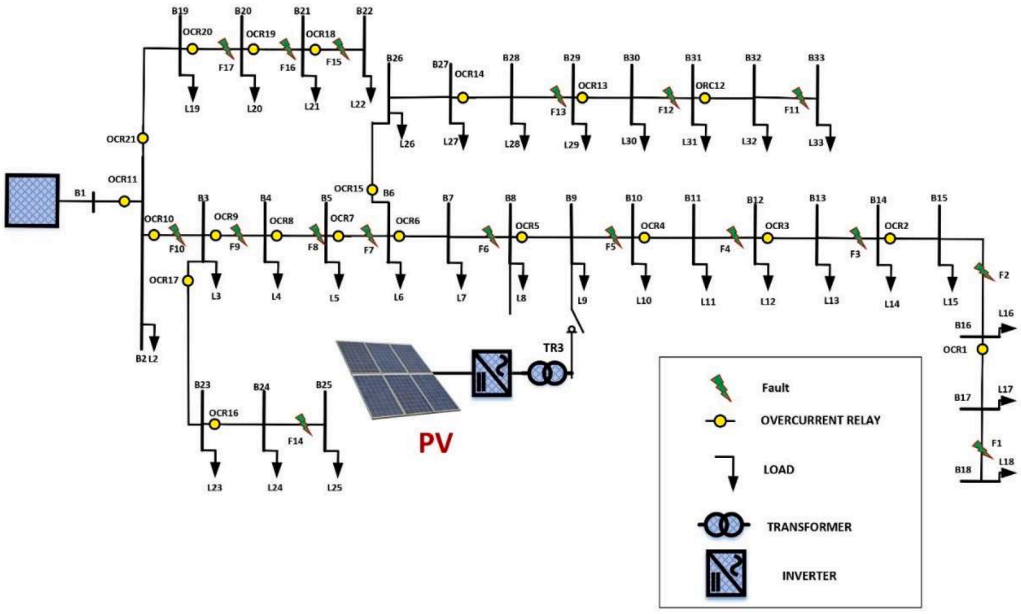

Fig. 10. IEEE 33-Bus network.

PVOCR (black line) initially starts with a significantly higher operation time, around 80, compared to SOCR (green line) and VOCR (blue line), which begin at approximately 40 and 30, respectively. Despite this, PVOCR demonstrates superior performance by converging more rapidly within the first 50 iterations, drastically reducing its operation time. By around the 100th iteration, PVOCR's operation time stabilizes around 20, matching the performance of SOCR and VOCR.

In addition, SOCR and VOCR also exhibit rapid convergence, with SOCR reducing its operation time to about 20 within the first 100 iterations, slightly faster than VOCR, which reaches the same stable operation time a bit later. However, both SOCR and VOCR maintain this steady state beyond the initial convergence phase. In contrast, PVOCR, despite its higher initial computational cost, quickly achieves and sustains a similar steady-state performance, demonstrating its efficiency. In summary, while SOCR and VOCR start with lower initial operation times and quickly reach stable performance, PVOCR, despite its high initial operation time, converges more rapidly and achieves comparable long-term performance. This makes PVOCR the better algorithm, especially considering its ability to swiftly reduce operation time and maintain efficiency.

- IEEE 9 mesh network

To investigate the mesh network coordination issues, an IEEE 9 mesh network with DG, as described in Fig. 12. This investigation aims to validate the protection scheme's transferability across different network configurations.

The SOCR, VOCR and PVOCR coordinating schemes are tested and

Table 13
Initial Time Multiplier Setting (TMS) for each OCR.

OCR	TMS		
	SOCR	VOCR	PVOCR
OCR1	0.01	0.01	0.01
OCR2	0.08519887	0.437016172	0.129102216
OCR3	0.171690702	0.565391542	0.218664955
OCR4	0.266396229	0.930173948	0.342936253
OCR5	0.34288601	1.340371956	0.40539648
OCR6	0.438603782	0.862609562	0.423740034
OCR7	0.543092439	0.882108221	0.51233212
OCR8	0.669904355	1.279737187	0.644314027
OCR9	0.810906127	1.697257798	0.758233636
OCR10	0.958354587	1.610452209	0.821768317
OCR11	0.886296108	1.832886322	0.831916472
OCR12	0.01	0.01	0.01
OCR13	0.09497774	0.491375524	0.140355576
OCR14	0.188215322	0.681643032	0.245482127
OCR15	0.291783427	0.663277081	0.330352542
OCR16	0.01	0.01	0.01
OCR17	0.130921389	0.340684436	0.154626074
OCR18	0.010328569	0.01	0.01000025
OCR19	0.126952253	0.603150122	0.172415992
OCR20	0.252281039	0.843175617	0.308326261
OCR21	0.407460075	0.964372479	0.422183038

Table 14
The tripping time results for SOCR, VOCR and PVOCR schemes at the IEEE-30 BUS network under Control 4.

Fault location	Relays	Fault current (A)	SOCR	VOCR	PVOCR
F1	OCR1	561	0.039894306	0.021320131	0.004600899
	OCR2	561	0.33989498	0.321320267	0.304601415
F2	OCR2	723	0.295551658	0.231827148	0.149031514
	OCR3	723	0.59558855	0.531828579	0.44903419
F3	OCR3	865	0.545102553	0.451268346	0.302427016
	OCR4	865	0.845784094	0.751270852	0.602443132
F4	OCR4	942	0.81292757	0.476461335	0.204223219
	OCR5	826	1.112935927	0.776461342	0.564524474
F5	OCR5	887	1.075833474	0.701029792	0.450423057
	OCR6	887	1.376155974	1.002042499	0.750423509
F6	OCR6	1080	1.259798428	0.865229648	0.522192864
	OCR7	1080	1.55992043	1.170338019	0.822204833
F7	OCR7	1772	1.284800601	0.81590038	0.32125459
	OCR8	1772	1.584801142	1.116237952	0.621255931
F8	OCR8	2401	1.428945364	0.832967461	0.296550749
	OCR9	2401	1.72971043	1.135635722	0.596766242
F9	OCR9	2786	1.649912169	0.972232518	0.402853348
	OCR10	2786	1.949918545	1.272261482	0.70356698
F10	OCR10	3290	1.85398674	1.091226916	0.448572243
	OCR11	3290	2.154021094	1.391490612	0.749379867
F11	OCR12	699	0.035303868	0.01828603	0.003510426
	OCR13	699	0.335308164	0.318298733	0.303511642
F12	OCR13	841	0.305616968	0.256685457	0.185245329
	OCR14	841	0.605634498	0.556686499	0.485259699
F13	OCR14	1058	0.545439147	0.448900954	0.286369873
	OCR15	1058	0.84557464	0.749075632	0.586441188
F14	OCR16	1556	0.024810069	0.018284559	0.005387368
	OCR17	1556	0.324816873	0.318928946	0.305428345
F15	OCR18	1415	0.026569336	0.015285464	0.002946675
	OCR19	1415	0.32657352	0.315292622	0.302946788
F16	OCR19	1715	0.303888003	0.263537707	0.191569845
	OCR20	1715	0.603889883	0.563742476	0.491771556
F17	OCR20	2174	0.556045124	0.471325339	0.300475237
	OCR21	2174	0.898070616	0.772022931	0.708006236

evaluated over different fault scenarios in terms of locations and type. Table 16 shows the fault currents in various scenarios, including different fault locations, and PV control modes. For instance, in Fault F1, under Control 4, OCR3 registered a lower fault current (4561 A) compared to other controls, where Control 1 registered a maximum current (4815 A). This variation in the fault current contribution from

Table 15
The total tripping time results for SOCR, VOCR and PVOCR schemes at the IEEE-30 BUS network under Control 1,2,3 and 5.

Control	TMS		
	SOCR	VOCR	PVOCR
1	30.963	20.572	17.266
2	32.556	20.231	37.687
3	49.484	21.198	17.385
5	34.058	21.019	18.179

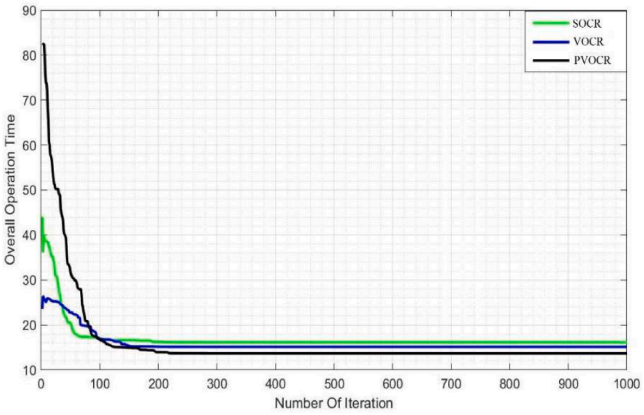

Fig. 11. Convergence and computing Time for SOCR, VOCR, and PVOCR.

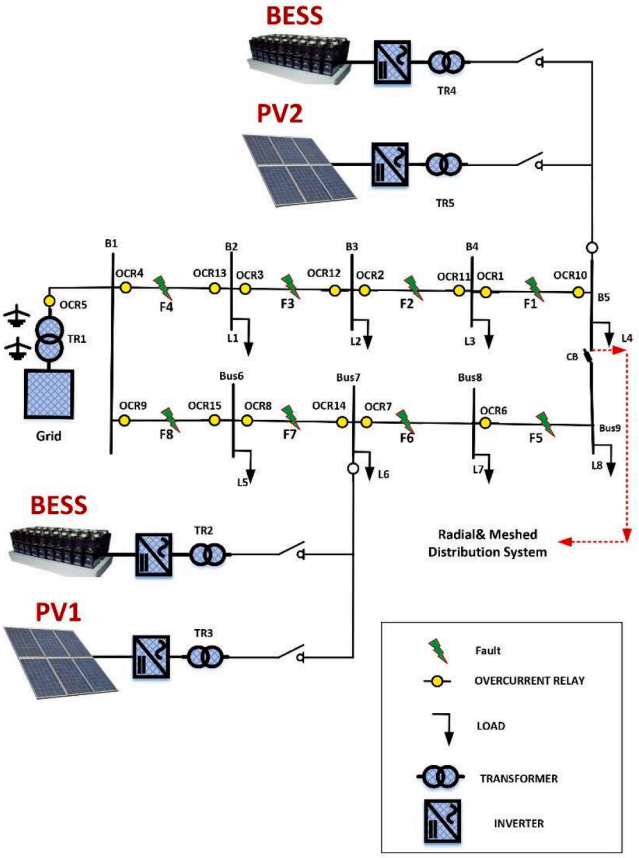

Fig. 12. IEEE 9-Bus mesh network.

Table 16
The fault currents under different PV control modes and fault locations for mesh network.

Fault location	Relays Pairs	Control 1	Control 2	Control 3	Control 4	Control 5
		Fault current (A)				
F1	OCR1	2877	2862	2858	2802	2867
	OCR2	2877	2862	2858	2802	2867
	OCR10	4302	4160	4022	3209	3654
F2	OCR2	3755	3724	3657	3598	3733
	OCR3	3755	3724	3657	3598	3733
	OCR11	3403	3245	2483	2486	3053
	OCR10	3403	3245	2483	2486	3053
F3	OCR3	4815	4765	4748	4561	4778
	OCR4	4815	4765	4748	4561	4778
	OCR12	2567	2434	2340	1795	2318
	OCR11	2567	2434	2340	1795	2318
F4	OCR4	6180	6010	5881	5805	6106
	OCR5	6169	6010	6269	6318	6225
	OCR13	1720	1161	1045	1067	1146
	OCR12	1720	1161	1045	1067	1146
F5	OCR6	3324	3257	3218	2937	3231
	OCR7	3324	3257	3218	2937	3231
F6	OCR7	4260	4169	4066	3742	4078
	OCR8	3388	3399	3354	3471	3426
F7	OCR8	4525	4509	4390	4446	4511
	OCR9	4525	4509	4390	4446	4511
	OCR14	2115	2939	2236	1941	2364
F8	OCR9	5856	5822	5559	5681	5814
	OCR5	6259	6269	6350	6334	6300
	OCR15	2274	2096	801	1209	1655
	OCR14	2274	2095	801	1209	1655

the PV inverter, dependent on the control model, adds complexity to the development of an optimal OCR coordination scheme. The fault current contributions from PV systems are directly affected by V_P^+, which varies depending on the location of the PV system and the control modes used. Table 17 presents the V_P^+ values for two PV farms (PV1 and PV2) under various fault locations and inverter control modes. PV2 consistently shows higher voltage levels compared to PV1 at fault locations F1, F2, F3, and F4 due to its proximity to these faults. In contrast, PV1 demonstrates higher voltage levels than PV2 at fault locations F5, F6, F7, and F8, as it is nearer to these faults.

To evaluate the effectiveness of the proposed OCR protection schemes (SOCR, VOCR, and PVOCR), optimal OCR settings were established for the power mesh network. Table 18 presents the optimal OCR settings for SOCR, VOCR, and PVOCR under three-phase fault conditions and different PV inverter control modes. Secondly, Table 6 also compares the total tripping times of the OCR schemes (SOCR, VOCR, and PVOCR), focusing on the tripping times for primary and backup OCR pairs during three-phase faults. The proposed PVOCRS approach demonstrates superior performance, achieving the shortest tripping time compared to the benchmark SOCR and VOCR approaches in all PV inverter control modes. For instance, the overall tripping times for SOCR, VOCR, and PVOCR are 23.1, 18.33, and 16.67 s, respectively, in Control 4 mode.

Table 17
The PV systems voltage (V_P^+) under different PV controls and fault locations for mesh network.

Fault location	Relays Pairs	Control 1	Control 2	Control 3	Control 4	Control 5
		V_P^+ (p.u)				
F1	PV1	0.1916	0.1612	0.1546	0.0479	0.0694
	PV2	0.3168	0.288	0.2753	0.2153	0.2828
F2	PV1	0.2563	0.2232	0.0724	0.1177	0.185
	PV2	0.3603	0.3293	0.302	0.245	0.3264
F3	PV1	0.2979	0.2627	0.2439	0.1489	0.2345
	PV2	0.3642	0.3311	0.3134	0.2364	0.3267
F4	PV1	0.3031	0.2661	0.0913	0.137	0.2263
	PV2	0.3269	0.2917	0.2465	0.1824	0.2688
F5	PV1	0.1916	0.1612	0.1646	0.0479	0.069
	PV2	0.3168	0.288	0.2753	0.215	0.2828
F6	PV1	0.2417	0.21	0.0629	0.114	0.1712
	PV2	0.263	0.2331	0.2199	0.1539	0.2115
F7	PV1	0.2687	0.2364	0.085	0.1416	0.257
	PV2	0.1916	0.1612	0.1546	0.04	0.069
F8	PV1	0.2888	0.2527	0.0698	0.133	0.207
	PV2	0.2395	0.205	0.0239	0.08	0.1349

5. Conclusions

This research addressed challenges in the protection system of distribution networks with inverter-interfaced distributed generators (IBDGs). The study investigates fault characteristics and fault current contributions from different PV systems under various control strategies, emphasizing the impact of control strategies and fault locations on protection system behaviour during faults, observed in a 9-bus IEEE network with two 7 MVA PV farms and two 0.6 MVA BESS. The results highlight how these parameters affect how overcurrent relay (OCR) protection methods in developing power systems coordinate and identify misoperation events. This research highlights the importance of modifying protection strategies to take into consideration IBDG dynamics under different fault scenarios. It makes clear how crucial it is to take PV contribution changes based on the control mode into account for optimal OCR coordination. Furthermore, optimal coordination schemes using current-voltage characteristics (PVOCR) are evaluated and compared to standard SOCR and modern VOCR schemes under different inverter control modes. The Water Cycle Optimization algorithm (WCA) was used to solve the OCR coordination problem under the potential impact of PV inverter control strategies on fault contribution and relay setting. The findings indicate that the PVOCR approach significantly outperforms the benchmark SOCR and VOCR schemes, achieving a minimum tripping time of 13.67 s compared to 16.13 s for SOCR and 15.12 s for VOCR. In summary, this study improves the understanding of PV inverter control strategies and OCR protection in dynamic power systems. The paper also presents a fast-response OCR technique that takes into account different inverter control modes by utilizing the PVOCR approach. When it comes to five control scenarios, the suggested PVOCR technique offers a creative and effective solution that shows optimal coordination and shorter operating times than other methods and without misoperation events.

Ethical approval

Not applicable.

Funding

The authors extend their appreciation to the Deanship of Research and Graduate Studies at King Khalid University for funding this work through Large Research Project under grant number RGP2/238/45.

CRediT authorship contribution statement

Feras Alasali: Writing – review & editing, Writing – original draft, Validation, Supervision, Methodology, Formal analysis, Data curation. **Hamza Albayadrah:** Validation, Software, Methodology, Investigation, Formal analysis, Data curation, Conceptualization. **Naser El-Naily:** Writing – original draft, Validation, Resources, Methodology, Investigation, Formal analysis, Data curation. **Hassen Loukil:** Writing – review & editing, Visualization, Validation, Supervision, Resources, Investigation, Funding acquisition. **William Holderbaum:** . **Aymen Flah:** Writing – review & editing, Visualization, Validation, Resources, Methodology, Data curation. **Abdelaziz Salah Saidi:** Writing – review & editing, Visualization, Validation, Supervision, Resources, Methodology, Investigation.

Table 18
TMS and overall tripping time results under different PV control modes in mesh network.

OCR	Control 1			Control 2			Control 3			Control 4			Control 5		
	TMS														
	SOCR	VOCR	PVOCR	SOCR	VOCR	PVOCR	SOCR	VOCR	PVOCR	SOCR	VOCR	PVOCR	SOCR	VOCR	PVOCR
OCR1	0.010	0.010	0.010	0.010	0.010	0.010	0.010	0.010	0.010	0.010	0.10	0.010	0.010	0.010	0.010
OCR 2	0.1815	0.7331	0.229	0.162	0.802	0.21	0.18	0.708	0.239	0.175	0.702	0.229	0.178	0.752	0.276
OCR 3	0.379	1.12	0.423	0.329	1.101	0.43	0.34	1.18	0.443	0.342	1.185	0.433	0.345	1.225	0.462
OCR 4	0.546	1.33	0.616	0.509	1.408	0.60	0.534	1.534	0.616	0.518	1.547	0.626	0.514	1..397	0.629
OCR 5	0.504	3.067	0.715	0.49	1.795	0.731	0.546	1.866	0.742	0.522	3.257	0.757	0.523	3.00	0.790
OCR 6	0.010	0.010	0.010	0.010	0.010	0.010	0.010	0.010	0.010	0.010	0.01	0.010	0.010	0.010	0.010
OCR 7	0.19	0.670	0.21	0.164	0.62	0.234	0.187	0.643	0.229	0.177	1.22	0.261	0.178	0.689	0.222
OCR 8	0.32	1.52	0.42	0.31	1.13	0.422	0.365	1.13	0.405	0.339	1.601	0.466	0.315	1.177	0.448
OCR 9	0.42	1.679	0.54	0.446	1.33	0.560	0.460	1.322	0.533	0.47	1.760	0.554	0.420	1.321	0.576
OCR 10	0.259	2.21	0.60	0.207	1.209	0.654	0.200	1.299	0.6261	0.130	0.150	0.645	0.111	0.648	0.652
OCR 11	0.183	1.67	0.44	0.123	0.825	0.453	0.136	0.825	0.453	0.090	0.090	0.453	0.081	0.491	0.465
OCR 12	0.096	1.579	0.255	0.079	0.433	0.250	0.072	0.456	0.229	0.050	0.05	0.234	0.0476	0.235	0.295
OCR 13	0.010	0.01	0.010	0.010	0.010	0.010	0.010	0.01	0.010	0.010	0.010	0.010	0.010	0.010	0.010
OCR 14	0.089	1.50	0.250	0.0828	0.441	0.251	0.077	0.459	0.245	0.050	4.0	0.250	0.0523	0.230	0.250
OCR 15	0.010	0.010	0.010	0.010	0.010	0.010	0.010	0.010	0.010	0.010	0.01	0.010	0.010	0.010	0.010
Overall time (S.)	21.23	18.32	16.61	22.6	19.26	16.72	20.34	17.99	15.77	23.1	18.33	16.67	19..44	17.77	15..1

Declaration of competing interest

We confirm that this work is original and has not been published elsewhere, nor is it currently under consideration for publication elsewhere and the authors declare no conflict of interest. We also confirm that all authors have participated in drafting the article or revising it critically for important intellectual content; approval of the final version.

Data availability

Data will be made available on request.

Acknowledgment

We would like to thank The Hashemite University (Renewable Energy Center) and the University of Salford for their support in publishing this article.

Appendix A

Table A1
The TMS for IEEE 33-BUS network results under PV control 1.

	TMS		
OCR	SOCR	VOCR	PVOCR
OCR1	0.01	0.01	0.01
OCR2	0.07494677	0.507579687	0.129136713
OCR3	0.144244717	0.760866021	0.21872972
OCR4	0.2179558	1.301267329	0.343049477
OCR5	0.099929482	1.533038621	0.340573517
OCR6	0.127386219	1.729014733	0.379764807
OCR7	0.156877756	2.249999671	0.470752911
OCR8	0.202183784	3.936364405	0.607272904
OCR9	0.236254215	4.720491156	0.724277253
OCR10	0.271827911	5.155703206	0.797806812
OCR11	0.045708159	6	0.854611581
OCR12	0.01	0.01	0.014154637
OCR13	0.072952543	0.645223545	0.143682433
OCR14	0.140601134	1.018796345	0.247649354
OCR15	0.212855997	1.212939713	0.332051083
OCR16	0.01	0.01	0.010001294
OCR17	0.084029027	0.765137025	0.154894844
OCR18	0.01	0.01	0.010001469
OCR19	0.080010475	0.951419553	0.189010022
OCR20	0.153047525	1.627214973	0.32229566
OCR21	0.228185185	2.098624348	0.433547909

Table A2
The TMS for IEEE 33-BUS network results under PV control 2.

OCR	TMS		
	SOCR	VOCR	PVOCR
OCR1	0.01	2.126011396	0.01
OCR2	0.073843309	2.027279644	0.12911597
OCR3	0.171690702	1.539755956	0.218713905
OCR4	0.266396229	2.812954312	0.350053515
OCR5	0.34288601	2.367282421	0.344449848
OCR6	0.438603782	2.282037799	0.382801516
OCR7	0.543092439	2.716239911	0.473467982
OCR8	0.669904355	3.608892218	0.608427629
OCR9	0.810906127	4.444252455	0.725254591
OCR10	0.958354587	4.903542583	0.928194203
OCR11	0.886296108	5	0.936568526
OCR12	0.01	0.01	0.010007072
OCR13	0.09497774	4.679429309	0.140325293
OCR14	0.188215322	3.709606553	0.245510518
OCR15	0.291783427	4.945522075	0.241703741
OCR16	0.01	2.016837072	0.010000017
OCR17	0.130921389	2.503910375	0.154516211
OCR18	0.010328569	0.01	0.010009995
OCR19	0.126952253	2.173567404	0.172648884
OCR20	0.252281039	4.999722177	0.308442643
OCR21	0.407460075	4.603211742	0.422183038

Table A3
The TMS for IEEE 33-BUS network results under PV control 3.

OCR	TMS		
	SOCR	VOCR	PVOCR
OCR1	0.01	0.01	0.01
OCR2	0.06867486	0.54731898	0.129115212
OCR3	0.132821189	0.826700363	0.218678008
OCR4	0.157432164	1.621005981	0.34297916
OCR5	0.184888915	2.158897257	0.410929944
OCR6	0.212803941	2.132804864	0.42749766
OCR7	0.2448411	2.590338304	0.518680822
OCR8	0.277514004	3.497506955	0.654183692
OCR9	0.314437713	4.35067027	0.765017051
OCR10	0.350818779	4.831897848	0.827086932
OCR11	0.057465993	6.232812076	0.855555738
OCR12	0.01	0.013560716	0.010007072
OCR13	0.069169369	0.671767545	0.140362827
OCR14	0.131460947	1.08245626	0.245780114
OCR15	0.160357216	1.596706579	0.330801504
OCR16	0.01	0.01	0.010000017
OCR17	0.105719363	0.925986275	0.154197637
OCR18	0.01	0.01	0.01
OCR19	0.075440638	0.975109624	0.172392068
OCR20	0.108092208	1.863189251	0.308229301
OCR21	0.147840251	2.561044451	0.421626676

Table A4
The TMS for IEEE 33-BUS network results under PV control 5.

OCR	TMS		
	SOCR	VOCR	PVOCR
OCR1	0.01	0.01	0.01
OCR2	0.043494582	0.679848778	0.129113319
OCR3	0.079903687	1.10782409	0.218582358
OCR4	0.11828911	1.820554765	0.342943633
OCR5	0.104739036	2.206253324	0.400725908
OCR6	0.132591526	2.165444732	0.420605201
OCR7	0.162119464	2.617844205	0.50730945
OCR8	0.194802972	3.52078834	0.639555006
OCR9	0.229265962	4.740683739	0.752126125
OCR10	0.264041293	5.145770503	0.816820407
OCR11	0.044561205	5.443861769	0.845729229

(*continued on next page*)

Table A4 (*continued*)

OCR	TMS		
	SOCR	VOCR	PVOCR
OCR12	0.01	0.01	0.01
OCR13	0.047225036	0.78009909	0.140455757
OCR14	0.086179694	1.317317434	0.249305357
OCR15	0.129315027	1.69410352	0.333279777
OCR16	0.01	0.01	0.010000017
OCR17	0.054185074	0.882769553	0.1543236
OCR18	0.01	0.033317328	0.01
OCR19	0.053227754	1.08442068	0.172399088
OCR20	0.136117241	1.901957576	0.308111058
OCR21	0.181728548	2.553981157	0.422051568

References

[1] H.A. Abdel-Ghany, A.M. Azmy, N.I. Elkalashy, E.M. Rashad, Optimizing DG penetration in distribution networks concerning protection schemes and technical impact, Electr. Power Syst. Res. 128 (2015) 113–122.

[2] M.N. Naz, M.I. Mushtaq, M. Naeem, M. Iqbal, M.W. Altaf, M. Haneef, Multicriteria decision making for resource management in renewable energy assisted microgrids, Renew. Sustain. Energy Rev 71 (2017) 323–341.

[3] F. Alasali, H. Mustafa, A.S. Saidi, N. El-Naily, S. Abeid, W. Holderbaum, S. Saad, The recent development of protection coordination schemes based on inverse of AC microgrid: a review, IET Generat. Transmiss. Distribut. (2023), https://doi.org/10.1049/gtd2.13074.

[4] F. Alasali, S. Saad, A.S. Saidi, A. Itradat, W. Holderbaum, N. El-Naily, F. Elkuwafi, Powering up microgrids: a comprehensive review of innovative and intelligent protection approaches for enhanced reliability, Energy Rep. 10 (2023) 1899–1924.

[5] H. Yazdanpanahi, W. Li, W. Xu, A new control strategy to mitigate the impact of inverter-based DGs on protection system, IEEE Trans. Snart Grid 3 (3) (2012) 1427–1436.

[6] A.K. Singh, I. Hussain, B. Singh, Double-stage three phase grid- integrated solar PV system with fast zero attracting normalized least mean forth based adaptive control, IEEE Trans. Ind. Electr 65 (5) (2018) 3921–3931.

[7] K.A. Saleh, H.H. Zeineldin, A. Al-Hinai, E.F. El-Saadany, Optimal coordination of directional overcurrent relays using a new time–current–voltage characteristic, IEEE Transact. Power Deliv. 30 (2) (2014) 537–544.

[8] K.A. Saleh, M.S. El Moursi, H.H. Zeineldin, A new protection scheme considering fault ride through requirements for transmission level interconnected wind parks, IEEE Transact. Ind. Inform. 11 (6) (2015) 1324–1333.

[9] S. Jamali, H. Borhani-Bahabadi, Protection method for radial distribution systems with DG using local voltage measurements, IEEE Transact. Power Deliv. 34 (2) (2018) 651–660.

[10] M. Singh, A. Agrawal, Voltage–current–time inverse-based protection coordination of photovoltaic power systems, IET Generat. Transmiss. Distribut. 13 (6) (2019) 794–804.

[11] W.T. El-Sayed, M.A. Azzouz, H.H. Zeineldin, E.F. El-Saadany, A harmonic time-current-voltage directional relay for optimal protection coordination of inverter-based islanded microgrids, IEEE Trans. Smart Grid 12 (3) (2020) 1904–1917.

[12] P. Singh, A.K. Pradhan, A Local measurement based protection technique for distribution system with photovoltaic plants, IET Renew. Power Generat. 14 (6) (2020) 996–1003.

[13] P. Mishra, A.K. Pradhan, P Bajpai, Positive sequence relaying method for solar photovoltaic integrated distribution system, IEEE Transact. Power Deliv. 36 (6) (2020) 3519–3528.

[14] S. Chakraborty, S. Das, Communication-less protection scheme for AC microgrids using hybrid tripping characteristic, Electr. Power Syst. Res. 187 (2020) 106453.

[15] K.A. Saleh, M.-S. Ali, Harmonic directional overcurrent relay for islanded microgrids with inverter-based DGs, IEEE Syst. J. 15 (2) (2020) 2720–2731.

[16] M. Singh, A q component-based adaptive protection coordination optimisation using overcurrent relays in coordination with fuses for hybrid microgrid, IET Gener., Transmiss. Distribut. 15 (14) (2021) 2061–2074.

[17] F. Alasali, N. El-Naily, E. Zarour, S.M. Saad, Highly sensitive and fast microgrid protection using optimal coordination scheme and nonstandard tripping characteristics, Int. J. Electr. Power Energy Syst. 128 (2021) 106756.

[18] T.T. Hoang, Q.T. Tran, Y. Besanger, An advanced protection scheme for medium-voltage distribution networks containing low-voltage microgrids with high penetration of photovoltaic systems, Int. J. Electr. Power Energy Syst. 139 (2022) 107988.

[19] H. Ebrahimi, A. Yazdaninejadi, S. Golshannavaz, S. Teimourzadeh, An ENS-oriented voltage protection scheme for inverter-based generators in active distribution networks, IEEE Trans. Smart Grid 13 (4) (2022) 2639–2649.

[20] M.A. Gabr, R.A. El-Sehiemy, T.F. Megahed, Y. Ebihara, S.M. Abdelkader, Optimal settings of multiple inverter-based distributed generation for restoring coordination of DOCRs in mesh distribution networks, Electr. Power Syst. Res. 213 (2022) 108757.

[21] A. Saber, H.H. Zeineldin, T.H. El-Fouly, A. Al-Durra, Overcurrent protection coordination with flexible partitioning of active distribution systems into multiple microgrids, Int. J. Electr. Power Energy Syst. 151 (2023) 109205.

[22] T.M. Vala, V.N. Rajput, A.S. Al-Sumaiti, Investigating the performance of non-standard characteristics-based overcurrent relays and their optimum coordination in distributed generators connected networks, IET Generat. Transmiss. Distribut. 17 (2023) 2978–2995.

[23] W.H. Kim, W.K. Chae, J.W. Lee, H.M. Lee, C.K. Lee, Active TCC based protection coordination scheme for networked distribution system, Int. J. Electr. Power Energy Syst. 153 (2023) 109341.

[24] G.P. Santos, A. Tsutsumi, J.C.M. Vieira, Enhanced voltage relay for AC microgrid protection, Electr. Power Syst. Res. 220 (2023) 109310.

[25] F. Alasali, A.S. Saidi, N. El-Naily, M.A. Smadi, W. Holderbaum, Hybrid tripping characteristic-based protection coordination scheme for photovoltaic power systems, Sustainability 15 (2) (2023) 1540.

[26] E. Zarour, F. Alasali, O. Alsmadi, N. El-Naily, A new adaptive protection approach for overcurrent relays using novel nonstandard current-voltage characteristics, Electr. Power Syst. Res. 216 (2023) 109083.

[27] F. Özveren, Ö. Usta, A power based integrated protection scheme for active distribution networks against asymmetrical faults, Electr. Power Syst. Res. 218 (2023) 109223.

[28] J.M. Tripathi, S.K Mallik, An adaptive protection coordination strategy utilising user-defined characteristics of DOCRs in a microgrid, Electr. Power Syst. Res. 214 (2023) 108900.

[29] A. Barranco-Carlos, C. Orozco-Henao, J. Marín-Quintero, J. Mora-Flórez, A. Herrera-Orozco, Adaptive protection for active distribution networks: an approach based on fuses and relays with multiple setting groups, IEEE Access 11 (2023) 31075–31091.

[30] U.U. Uma, D. Nmadu, N. Ugwuanyi, O.E. Ogah, N. Eli-Chukwu, M. Eheduru, A Ekwue, Adaptive overcurrent protection scheme coordination in presence of distributed generation using radial basis neural network, Protect. Contr. Mod. Power Syst. 8 (4) (2023) 1–19.

[31] A. Assouak, R. Benabid, A new coordination scheme of directional overcurrent and distance protection relays considering time-voltage-current characteristics, Int. J. Electr. Power Energy Syst. 150 (2023) 109091.

[32] M. Taheri, R. Mohammadi, M. Ghotbi-Maleki, Optimal cable size selection in distribution network considering damage curve with variable fault clearing time of overcurrent relay, Electr. Power Syst. Res. 225 (2023) 109812.

[33] A. Soni, A. Mohapatra, S. Singh, Protection coordination in AC microgrid via novel voltage-supervised directional over-current relays, IEEE Transact. Power Deliv. (2024), https://doi.org/10.1109/TPWRD.2024.3368624.

[34] IEEE Std 1547–2018, IEEE Standard for Interconnection and Interoperability of Distributed Energy Resources with Associated Electric Power Systems Interfaces, IEEE SA, Piscataway, NJ, USA, 2018, pp. 1–138.

[35] F. Alasali, S.M. Saad, N. El-Naily, A. Layas, A. Elhaffar, T. Hussein, F.A. Mohamed, Application of time-voltage characteristics in overcurrent scheme to reduce arc-flash incident energy for safety and reliability of microgrid protection, Energies 14 (2021) 8074.